# Examining Alzheimer's Disease Modifiable Risk Factors: Impact of Physical Activity and Diet on Neuroanatomy and Behaviour in Mice

Cindy L. García,[1,2]†* Chloe Anastassiadis,[1,2,3]† Mila Urosevic,[4] Megan Park,[2] Daniel Gallino,[2] Gabriel A. Devenyi,[2,5] Yohan Yee,[2] M. Mallar Chakravarty[2,5]*

1 - McGill University - Integrated Program in Neuroscience., Montreal, QC, Canada;
2 - Cerebral Imaging Centre - Douglas Mental Health University Institute., Montreal, QC, Canada;
3 - Tanz Centre for Research on Neurodegenerative Diseases, Toronto, ON, Canada;
4 - Biological and Biomedical Engineering, McGill University., Montreal, QC, Canada;
5 - Department of Psychiatry, McGill University., Montreal, QC, Canada.
*Corresponding authors
†These authors contributed equally to this work

**Abstract**
Dementia, a global public health challenge, is significantly influenced by lifestyle factors such as obesity. This study examines the impact of obesity and intervention approaches—physical exercise, a low-fat diet, or both—on brain structure in a triple-transgenic mouse model of Alzheimer's disease (3xTgAD) and wild-type mice fed a high-fat diet. Volumetric and deformation-based morphometry analyses showed significant neuroanatomical differences related to genotype and a high-fat diet, particularly affecting the hippocampus and cerebellum. Diet and exercise interventions partially mitigate these effects. Volume changes were correlated with behavioural data, producing a unique brain-behaviour signature tied to intervention-driven neuroanatomy improvements. This pattern was correlated with gene expression patterns, identifying modules of genes related to metabolic processes such as glucose homeostasis and fatty acid transportation. Overall, interventions promote changes that seem to counteract some of the effects of a high-fat diet, influencing biological processes that support brain health.

**Teaser**
Physical activity and diet ameliorate some of the brain changes observed in mice fed a high-fat diet.

## Introduction

Dementia is a condition characterized by a severe cognitive decline that impacts the ability to perform tasks related to daily living (*1*) and will affect ~78 million people worldwide by 2030 (*2*). The growing number of cases is partly attributable to increasing life expectancy, as age is the main risk factor for neurodegenerative disorders (*3*). However, approximately 40% of dementia cases are attributable to modifiable lifestyle factors such as hypertension, smoking, alcohol consumption, physical inactivity, and obesity (*4*).

Strategies aimed at addressing obesity are acknowledged as effective methods for preventing a range of diseases, such as cancer, diabetes, and heart conditions (*5–7*). What's more, the Alzheimer's Association reported that weight management can lower the risk of cognitive decline (*8*), advocating for this approach in the prevention of dementia. Several studies have linked regular weight maintenance and physical activity with a lower risk of developing dementia (*9–12*). For instance, combining physical activity with a Mediterranean diet effectively lowers the risk of developing Alzheimer's Disease (AD), the most common form of dementia (*13*). Conversely, diets high in saturated fats increase inflammatory markers such as interleukin-6 (*14*), implicated in the pathogenesis of AD (*15*), highlighting the importance of dietary factors in dementia prevention.

Only a few studies have focused on studying the effects of obesity and intervention strategies at the neuroanatomical level. For instance, it has been shown that obesity is associated with lower gray matter volumes in regions including the frontal gyri, insula, and cerebellum (*16*, *17*). In previous work from our laboratory, an obesity-inducing high-fat diet led to widespread morphological changes, including a decline in hippocampal volume in the triple transgenic mouse model of Alzheimer's disease (3xTgAD) (*18*). In contrast, other studies have found larger volumes of gray matter, white matter, hippocampus, and cerebellum related to physical activity (*19–21*).

To date, there is no randomized clinical trial data that proves that any intervention can prevent dementia (*22*), emphasizing the need for further research to understand how risk factors and interventions affect the brain. Despite the growing body of literature, the effects of obesity and intervention strategies on the brain remain largely unexplored. The present study builds upon our previous work to investigate the effects of three intervention strategies —physical activity, low-fat diet, and the combination of both— in the 3xTgAD mice, and their wild-type (WT) counterparts, both fed a high-fat diet. We hypothesized that interventions would mitigate the effects of the high-fat diet on weight, behaviour, and brain anatomy on 3xTgAD and WT mice. To test our hypothesis, we collected longitudinal weight measurements, and T1-weighted (T1-w) magnetic resonance images (MRI) at two, four, and six months of age. Additionally, we performed memory tests (Morris water maze and novel object recognition tests) after the last

MRI scan. We then related the voxel-wise brain volume changes and the results obtained from memory tests using partial least squares analysis (PLS), a multivariate technique that produced a unique signature of the relationship between the two. The observed brain-behaviour signature prompted further investigation into putative biological mechanisms behind interventions through Spatial Gene Enrichment Analysis (SGEA). We found that intervention strategies counteracted some of the effects of a high-fat diet, particularly in the cerebellum and hippocampus, where they brought structural volumes closer to those observed in controls. These changes are related to biological processes such as glucose homeostasis and positive regulation of fatty acid transport, as identified by SGEA.

## Results

### Experimental Groups and Study Timeline

We have provided a detailed description of the groups in Materials and Methods, 'Experimental design'. Briefly, all mice were fed a standard diet from 0-2 months of age (Fig. 1, initial N=165). Then, mice were switched to a low-fat or high-fat diet from 2-4 months of age. 3xTgAD and WT mice that remained on a low-fat diet with no further intervention for the rest of the experiment will be referred to as Tg_control (N=16) and WT_control (N=15) respectively. From 4-6 months, mice on a high-fat diet were divided into four groups per genotype: Tg_Diet (N=16) and WT_Diet (N=17) were mice that received a low-fat diet intervention; Tg_Exercise (N=16) and WT_Exercise (N=18) received access to a wheel to test physical activity intervention; Tg_Both (N=10) and WT_Both (N=17) received a combined intervention involving physical activity and a low-fat diet; and Tg_HighFat (N=16) and WT_HighFat (N=15) are mice on a high-fat diet with no further intervention. T1-w MRI were acquired with isotropic voxel dimensions of 100 µm at 2, 4, and 6 months of age on a Bruker 7T scanner, and novel object recognition (NOR) and Morris water maze (MWM) tests were performed after the last scan to examine the impact of the intervention on memory tests relevant to dementia phenotypes.

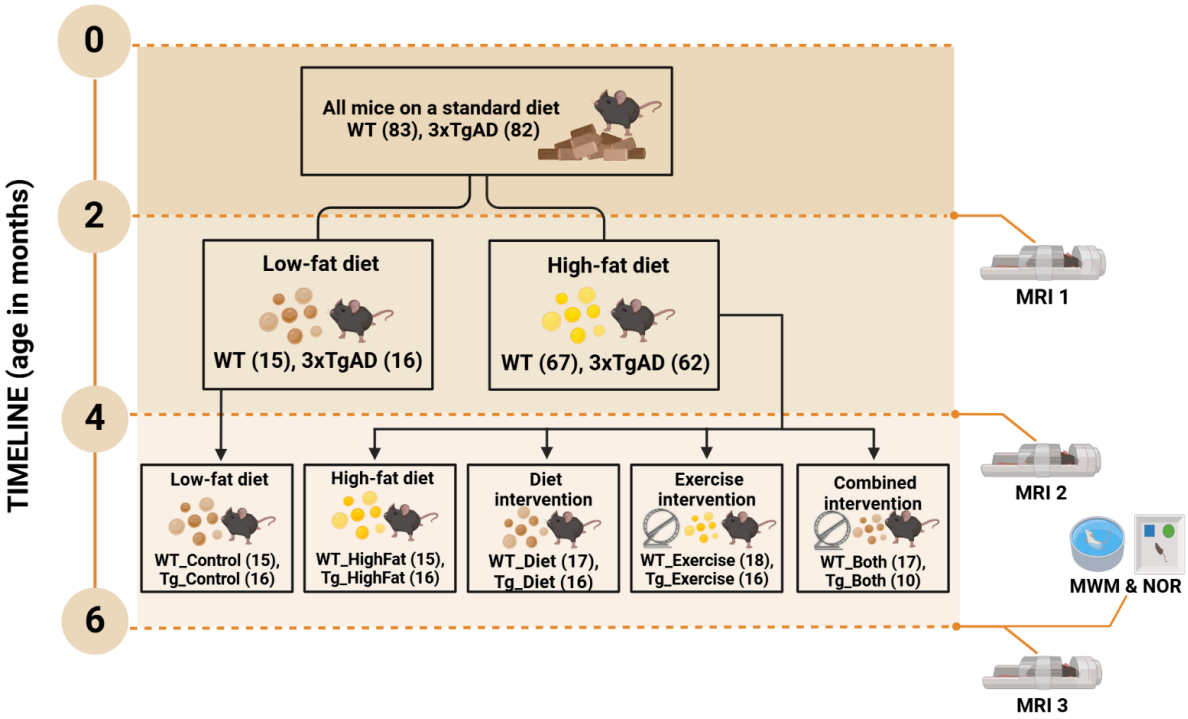


**Fig. 1. Experimental design.** For the first two months, all mice received a standard diet. From two to four months of age, mice were put on either a low-fat or high-fat diet. From four to six months of age, mice were placed in groups that received no intervention (WT_Control, Tg_Control, WT_HighFat, and Tg_HighFat groups), diet intervention (WT_Diet and Tg_Diet groups), physical activity (WT_Exercise and Tg_Exercise groups), or a combination of both (WT_Both and Tg_Both groups). T1w MRI scans were collected at two, four, and six months. behavioural tests (MWM and NOR) were performed after the last MRI scan. The numbers inside the parenthesis indicate the N of available mice at the end of each stage. MWM: Morris water maze, NOR: Novel object recognition test, MRI: Magnetic Resonance Images. Created in BioRender. Garcia, C. (2025) https://BioRender.com/q96h466.

**Intervention strategies affect the body weight of mice**

Mice were weighed weekly after the change in diet at two months of age and until the end of the experiment (N=157 mice, 18 measures of weight per mouse; see Fig. 1, and Materials and Methods, 'Experimental design'). The weight trajectories are plotted in Fig. 2-A. To analyze these trajectories, we used a linear mixed effects model (LME) including a third-degree polynomial for the interaction between group and weeks after the change in diet at 2 months of age, plus sex and a random intercept per mouse, using the WT_Control group as reference ($Weight \sim Group$*poly($Week$,3) + $Sex$ + ($1|ID$)). A third-degree polynomial can capture patterns in weight fluctuations that might not adhere to a linear path or a basic curve.

After the interventions started (black vertical line in Fig. 2-A), 3xTgAD and WT mice in the groups that received any form of intervention showed a decrease in weight by the end of the experiment, which demonstrates that the interventions not only counteracted the weight gain observed in high-fat diet groups but also adjusted weight trajectories to align more closely with the healthy control groups. The model identified a significant sex difference between males and females (p = 1.63e-05). We show the weight trajectories per genotype and sex (Fig. 2-B), where we observe higher weights for male mice in WT groups and higher weights for female mice in 3xTgAD groups, showing a genetic influence on weight dynamics across the sexes.

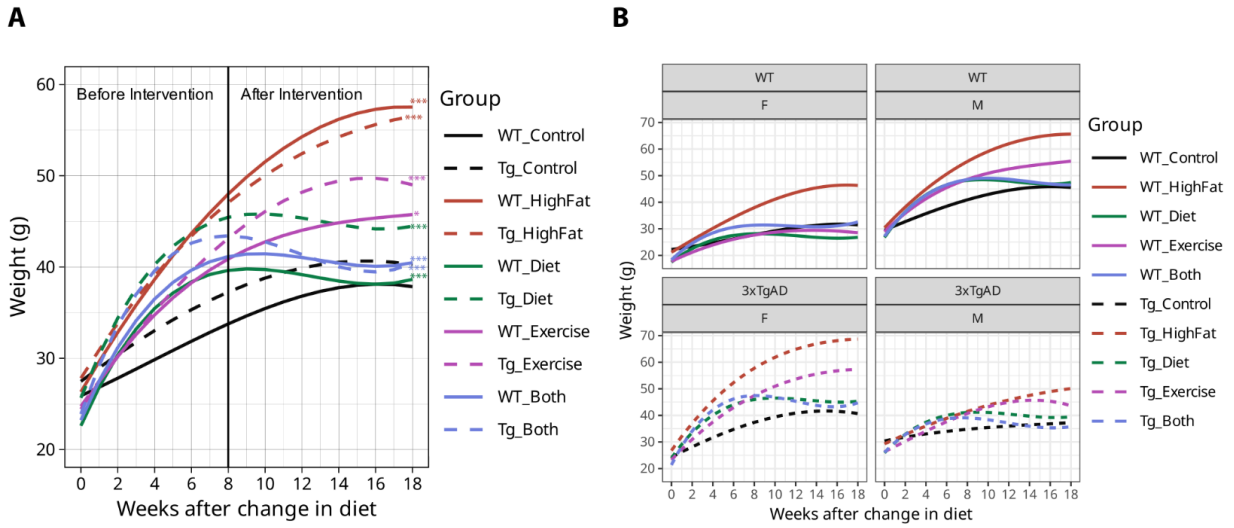


**Fig. 2. Weight trajectories per group and sex.** (**A**) Weekly measurements of weight are plotted per group. The black trajectory lines (solid and dashed) belong to the control groups (WT_Control, Tg_Control) and represent model-predicted weight trajectories. The vertical black line indicates the moment in which intervention strategies started. The x-axis shows weeks after the change in diet, and the y-axis shows the weight in grams. By the end of the experiment, interventions showed efficacy in lowering the weight of mice, some approaching levels close to those of the control group. Trajectories were modeled as described in the statistical analysis, 'weight' section, with a linear mixed effects model: *Weight* ~ *Group**poly(*Week*,3) + *Sex* + (*1*|*ID*), group-specific predictions are generated using a fitted model, where "Group" represents experimental conditions and "Week" represents the time since the diet change. Significance markers (*) indicate that the interaction between Group and Week significantly differs from the WT_Control reference group, based on the p-values of the interaction terms in the LME, see Statistical Analysis, 'Weight and behaviour' ('***' $p < 0.001$, '*' $p<0.05$). N=157 mice, with 18 weight measurements each. (**B**) Weekly measurements of weight are plotted per group by genotype and sex. The upper panel shows WT mice, females to the left (N=35), and males to the right (N=47). The bottom panel shows 3xTgAD mice females to the left (N=39), and males to the right (N=36).

**No observable group differences were found in memory performance**

After the last MRI scan, the NOR and MWM tests were performed (see Materials and Methods, 'behavioural tests'). With these tests, recognition and spatial memory were assessed for each group. The NOR test evaluates mice's behaviour when exposed to novel and familiar objects. Because mice prefer novelty, if the mouse remembers the familiar object, it will spend more time exploring the novel object (*23*). This test indirectly assesses recognition memory, which depends on the perirhinal cortex and dorsal hippocampus (*24*). In this work, the paradigm was ideal for assessing short-term memory (*23*). In contrast, the MWM assesses long-term spatial memory, which depends on the hippocampus (*25*). In the MWM test, mice are trained to find an escape platform in a tank filled with water. After the training, it is expected that mice remember the platform's location, and therefore, they should spend more time in this location during probe day (*25*).

Variables of interest for the MWM are Gallagher's cumulative measure (GCM) (*26*), calculated as the average cumulative distance from the platform, and the number of pass-throughs (passages above the previous platform location) (*27*). GCM reflects how well the animal learns and remembers the platform's location, with lower values indicating more efficient learning (i.e., the animal spends more time near the platform). The number of pass-throughs is an indicator of spatial memory, higher pass-through counts suggest that the animal has accurately learned and remembers the platform's location. Variables of interest for the NOR are the percentage of time spent in the boundary area around the novel and the percentage of time spent in the boundary of the familiar object. More time around the novel object suggests the animal is more interested in it, which is a sign of better recognition memory (*24*). Variables reported here represent variables of interest commonly reported in the literature for these tests.

MWM variables were analyzed with pairwise comparisons of group means as described in the section Statistical Analysis, 'Weight and behaviour'. In this work, we did not find any significant differences when comparing the GCM of mice (Fig. S1-A). For the number of pass-throughs, we found one significant difference between Tg_HighFat and Tg_Diet ($p = 0.0035$; Fig. S1-B), with Tg_HighFat mice having a higher number of pass-throughs, meaning a better performance when compared to Tg_Diet.

When comparing the percentage of time spent in the boundary area around the novel and the percentage of time spent in the boundary of the familiar object, we did not find any differences for any of the groups (Fig. S1-C).

**Volumetric effects of genotype, high-fat diet, and interventions**

To assess the effects of genotype, high-fat diet, and interventions on brain anatomy, we applied a hierarchical LME model to the 182 regional volumes derived from the MAGeT brain segmentation algorithm using the Dorr-Steadman-Ullmann-Richards-Qiu-Egan (DSURQE) mouse brain atlas (*28–31*), as described in Materials and Methods, 'Volumetric analysis'. We used brain scans collected at 2, 4, and 6 months of age (see Materials and Methods, 'Experimental design'). The model included an interaction between group and age in days, with age modeled as a quadratic term, sex as an independent variable, and a random intercept per mouse (model: $Volume \sim Group*\text{poly}(Age,2) + Sex + (1|ID)$). Modeling age as a quadratic term allows the model to capture non-linear volumetric trajectories (*32*). All model outputs were corrected for multiple comparisons at a 10% False Discovery Rate (FDR) threshold (*33*).

Supplementary results, 'Volumetric analysis' show the comparison between 3xTgAD and WT mice in the low-fat diet groups (Tg_Control vs WT_Control) with significant wide-spread volumetric changes (genotype effect); while a high-fat diet and intervention strategies caused significant differences mainly in the cerebellum on WT mice but not on 3xTgAD mice (Fig. S2-4). These findings underline the sensitivity of volumetric analyses, which may miss subtle changes, such as minor atrophy or minor recovery, potentially underestimating biologically significant effects in 3xTgAD mice, motivating our next approach.

**Deformation Based Morphometry identifies similar patterns of local brain changes**

Our previous volumetric results allowed us to gain insight into the effects caused by the high-fat diet and intervention strategies. Our results suggest that all effects are stronger in WT groups. However, analysis at the level of regional volumes may not capture subtle brain changes happening at a smaller scale. To capture finer changes agnostic of predefined regions, we performed deformation-based morphometry (DBM) analysis (see Materials and Methods, 'Deformation Based Morphometry analysis'). This technique assesses structural brain differences by quantifying volumetric changes encoded by the deformations required to align individual brain images to a common template without the constraints of an anatomical prior. Voxel-wise deformations are assessed through the Jacobian determinant, which is a measure of volume contraction or expansion relative to the template (here, the population average) (*34*).

Positive Jacobian values indicate local expansion in the sample compared to the population average, while negative values indicate local contraction in the sample compared to the population average. DBM has been used previously in our group to study morphological changes in the 3xTgAD (*35*), 3xTgAD receiving a high-fat diet (*18*), and neurodegeneration in Parkinson's and frontotemporal dementia (*36–38*). LME models were conducted at each voxel. The model analyzed the logged Jacobian, with an interaction between group and age in days

(modeled as a quadratic polynomial), and sex, along with a random intercept for each mouse (model: *log-transformed Jacobian determinant* ~ *Group**poly(*Age*,2) + *Sex* + (*1*|*ID*)). Data from all time points were included, and results were corrected for multiple comparisons with FDR at a 10% threshold. Here we present the linear term of the interaction between group and age (Fig. 3); while statistically significant in some highly localized regions, the quadratic interaction term shows localized effects in some cortex areas and olfactory bulbs (Fig. S5).

Our DBM results are summarized in Fig. 3; where the linear term for the interaction between Tg_Control versus WT_Control (genotype effect) shows widespread significant differences in the cerebellum, hippocampus, caudoputamen, cortex, and olfactory bulbs. The subsequent section of the figure highlights the effects of a high-fat diet, which again shows impacts in the cerebellum as well as the hippocampus and caudoputamen, with no major significant effects seen in 3xTgAD mice, consistent with the volumetric analysis. These results indicate that the high-fat diet has effects at the voxel level, particularly pronounced in WT mice. On the other hand, the diet intervention effect indicates statistically significant differences in the cerebellar hemispheres in both genotypes, while physical activity has a significant impact on the hippocampus for both genotypes. Finally, the section analyzing combined interventions indicates significant differences in the cerebellum for both genotypes and in the hippocampus specifically for WT mice. No significant differences were observed between the sexes in any of the comparisons.

Overall, these results confirm that genotype has an effect with a particular pattern that spreads all over the cortex, cerebellum, and hippocampus. A similar pattern is observed as a result of feeding WT mice a high-fat diet. Each intervention strategy exhibits effects, particularly pronounced in the cerebellar regions, with exercise being the sole intervention that influences the hippocampus in both genotypes. Moreover, the DBM analysis allowed us to uncover effects resulting from intervention strategies in 3xTgAD mice that were not detectable at the volumetric level.

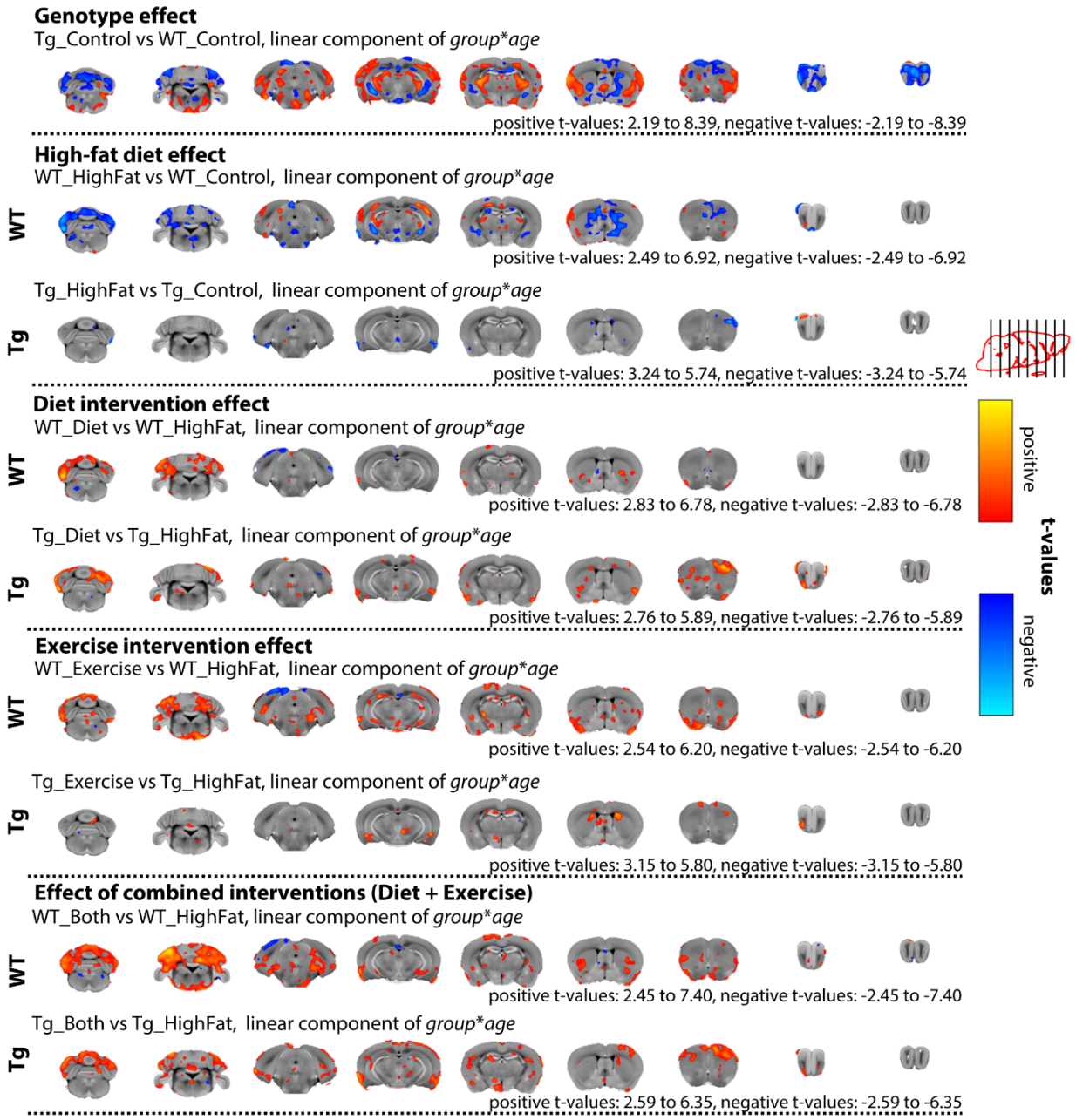


**Fig. 3. Brain volume changes of the group by age in days interaction as determined by voxel-based deformation analysis.** The t-statistic maps show the linear term of the significant interaction between group and age thresholded at 10% FDR, overlaid on the population average. Model: *log-transformed Jacobian determinant* ~ *Group**poly(*Age*,2) + *Sex* + (*1*|*ID*). N = 152 mice. FDR: False Discovery Rate.

**Peak-voxel trajectories reveal intervention strategies influence local brain structure**

Thus far, both volumetric and DBM analysis showed statistical effects caused by genotype, high-fat diet, and intervention strategies. To understand the volumetric changes underlying these statistical effects, and the direction of those changes, we selected peak voxels (voxels with a highly significant t-value) from the statistical maps produced by DBM analysis to uncover voxel-wise trajectories. In Fig. 4, the left images show the statistical maps on top of the population average, and the t-value and coordinates of the selected peak voxel. The middle graphs display the longitudinal trajectories of logged Jacobian values, and the right graphs present scatter plots, medians, and p-values from group comparisons at the third time point, offering a clearer view of the final differences observed by the end of the experiment.

Fig. 4 illustrates the genotype effect through significant peak voxels identified in two brain regions: the hippocampus (A) and the cerebellum (B). In these plots, we can see that both regions show significant genotype-related differences in structural changes over time with 3xTgAD groups generally maintaining lower Jacobian values than WT, which indicates a trend for a smaller volume. Exercise and diet appear to mitigate the structural deficits seen in Tg_HighFat, as their trajectories shift toward WT-like values, surpassing Tg_Control values. The graphs displayed on the right, which only present the values from the third time point, indicate trends that imply possible rescue effects resulting from the intervention strategies.

We notice this once more when examining peak voxels that emphasize the impacts of a high-fat diet. In the case of the hippocampus (Fig. 5-A), any intervention brings the Jacobian value closer to that of the WT_Control group, and it does so in a stepwise manner, with WT_Both having the closest Jacobian values to WT_Control, still showing a significant difference ($p=0.017$). For the cerebellar changes (Fig. 5-B) the three groups that received an intervention have a Jacobian value not significantly different from the WT_Control ($p>0.05$), this suggests that intervention strategies effectively rescue the changes caused by the high-fat diet in WT mice. In the bottom panel (high-fat diet effect on transgenic mice) we see the peak voxel trajectory selected from the cerebellar region. Again, intervention strategies push the trajectory away from that of the Tg_HighFat with no significant differences with Tg_Control ($p>0.05$).

Lastly, we show peak voxels obtained for each genotype for the effects of the combined intervention (physical activity and diet) against mice that didn't receive any intervention (Fig. 6). In WT mice, the cerebellum peak voxel shows a Jacobian value trend where WT_Both surpasses WT_Control, indicating a potential enhancement of brain structure beyond baseline levels. Similarly, in transgenic mice, the hippocampus peak voxel demonstrates a recovery trend, with intervention strategies restoring values to levels comparable to Tg_Control, and Tg_Both even exceeding Tg_Control. These findings suggest that the combined intervention may not only mitigate structural deficits but also promote improvements beyond control levels in specific brain

regions. The broader implications of these trends will be explored further in the discussion. Additional trajectories for groups receiving diet or physical activity are provided in Fig. S6-7, where we observed the same rescue effect.

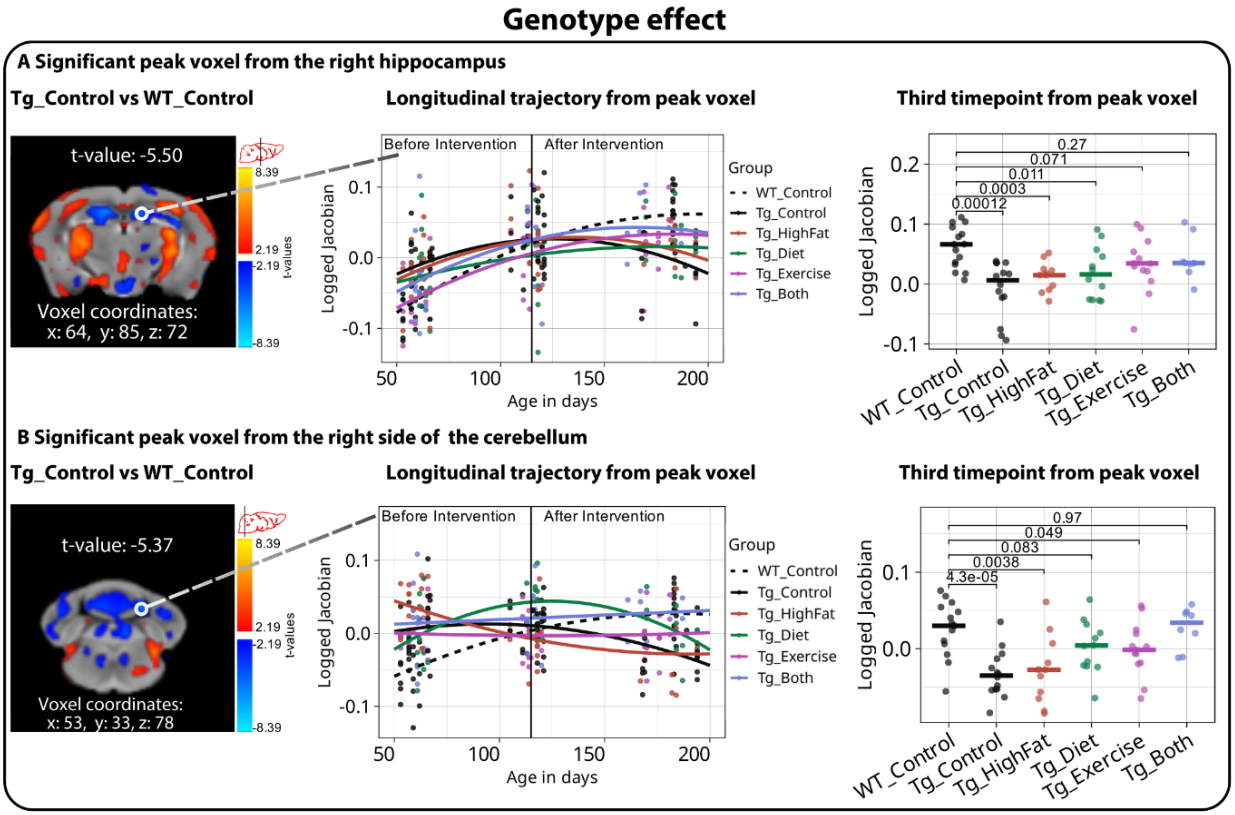


**Fig. 4. Trajectories of significant peak voxels identified for the genotype effect.** The figure shows two peak voxels selected from the significant difference between Tg_Control and WT_Control, which highlights the genotype effect on the hippocampus (**A**) and cerebellum (**B**). The left images show the statistical maps of the interaction between the group and age in days thresholded at 10% FDR and the regions from which peak voxels were selected; the middle graphs show the longitudinal trajectory of the Jacobian values of the selected peak voxels; and the right-sided graphs show the Jacobian values of the same peak voxels for the third time point to highlight group trends where p-values were obtained from a t-test corrected for multiple comparisons with FDR. FDR: False discovery rate (see Statistical Analysis, 'Volumetric and deformation-based analyses').

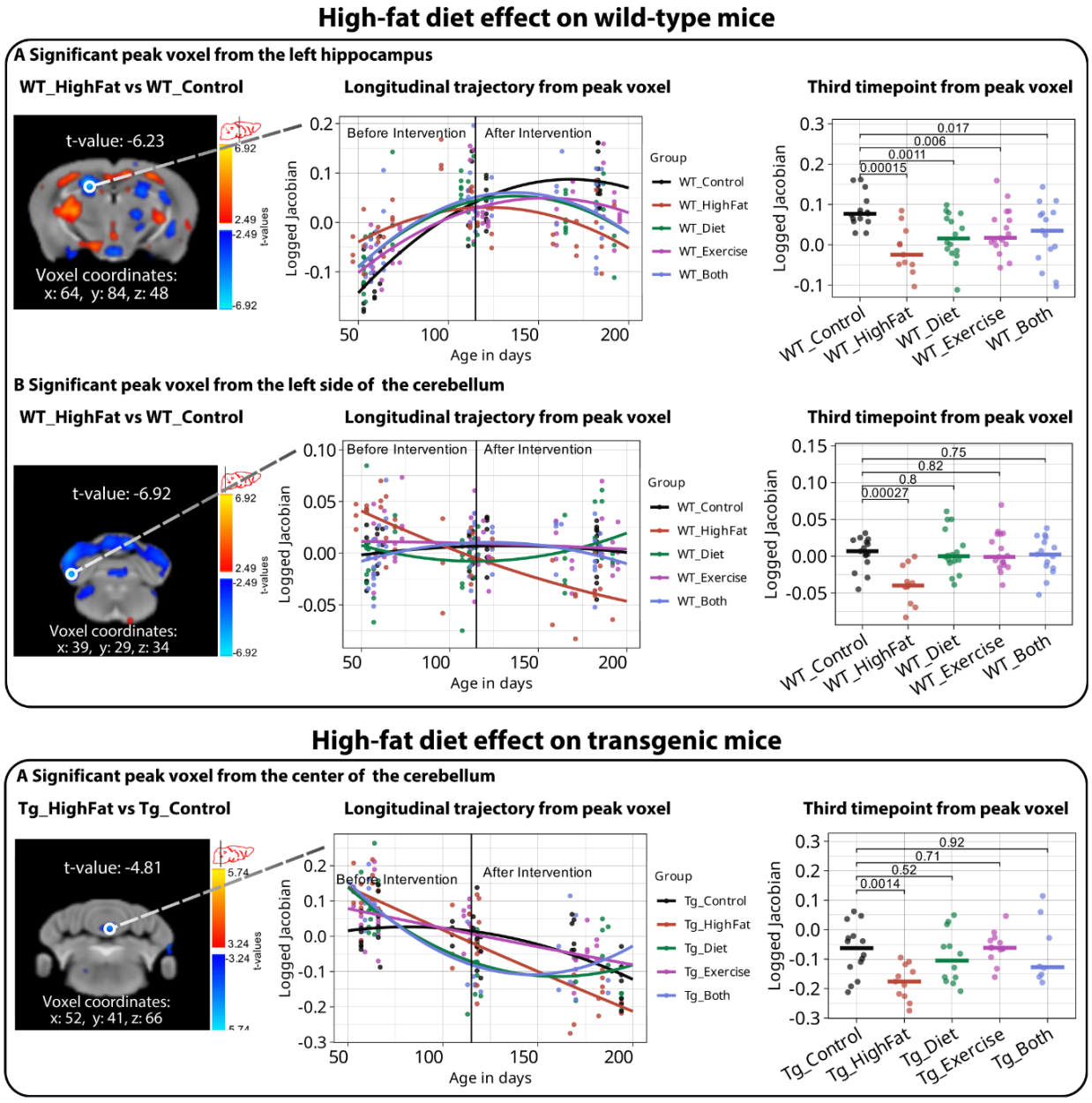


**Fig. 5. Trajectories of significant peak voxels identified for the high-fat diet effect.** The figure shows two peak voxels selected from the significant difference between WT_HighFat and WT_Control (top **A-B**), and one peak voxel selected from the comparison between Tg_HighFat vs. Tg_Control (bottom **A**) which highlights the effect of the obesity-inducing high-fat diet per genotype. The left images show the statistical maps of the interaction between the group and age in days thresholded at 10% FDR and t-values, and coordinates from which peak voxels were selected; the middle graphs show the longitudinal trajectory of the Jacobian values of the selected peak voxels; and the right-sided graphs show the Jacobian values of the same peak voxels for the third time point to highlight group trends where p-values were obtained from a

t-test corrected for multiple comparisons with FDR. FDR: False discovery rate (see Statistical Analysis, 'Volumetric and deformation-based analyses').

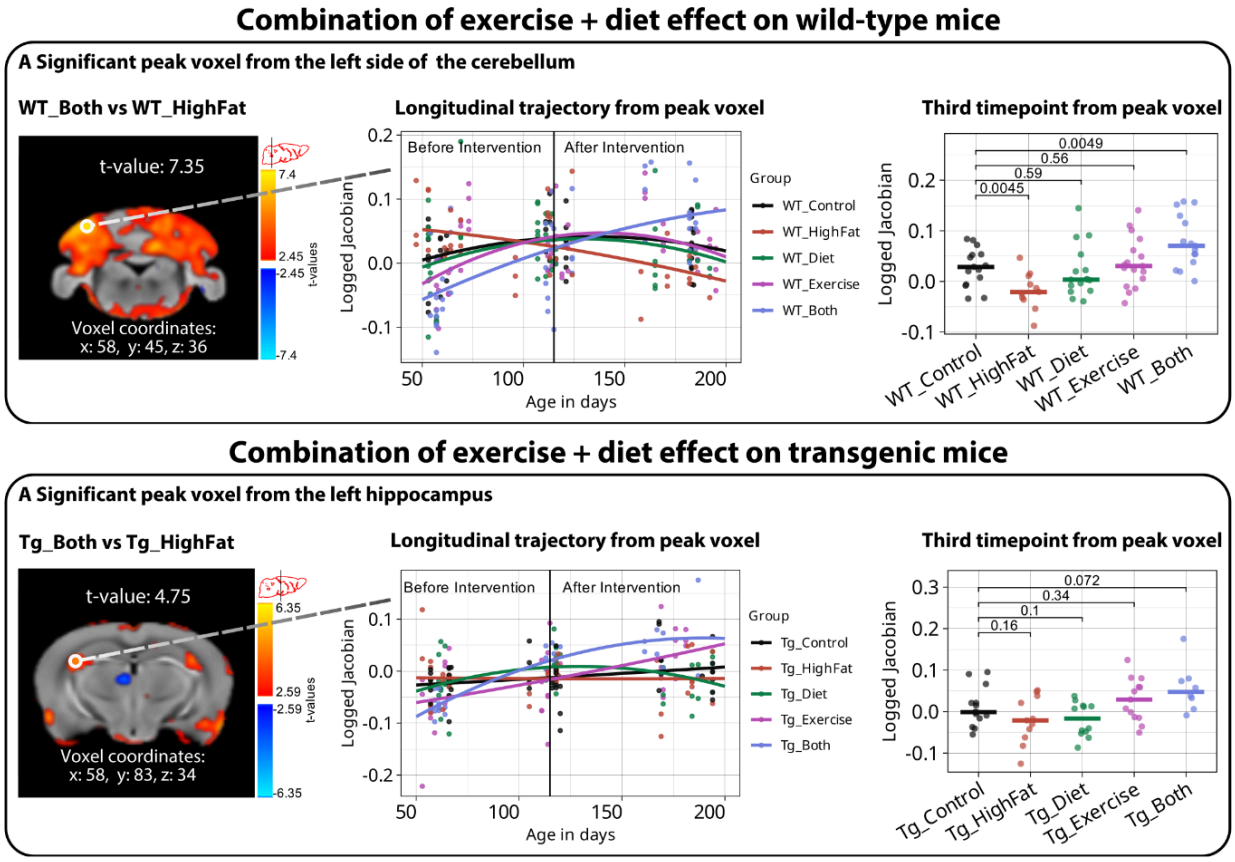


**Fig. 6. Trajectories of significant peak voxels identified for the combined interventions.** The figure shows a peak voxel selected from the cerebellar region from the significant difference between WT_Both and WT_HighFat (top-**A**), and another peak voxel selected from the left hippocampus from the comparison between Tg_Both vs. Tg_HighFat (bottom), which highlights the effect of the combined intervention. The left images show the statistical maps of the interaction between the group and age in days thresholded at 10% FDR, the t-values, and coordinates from which peak voxels were selected; the middle graphs show the longitudinal trajectory of the Jacobian values of the selected peak voxels; and the right-sided graphs show the Jacobian values of the same peak voxels for the third time point to highlight group trends where p-values were obtained from a t-test corrected for multiple comparisons with FDR. FDR: False discovery rate (see Statistical Analysis, 'Volumetric and deformation-based analyses').

**A signature of covariance between neuroanatomical changes and interventions**

Given the complexity of our data, which includes several groups, thousands of voxels, and over 30 behavioural variables, we utilized Partial Least Squares (PLS) analysis, a multivariate method that identifies relationships that explain shared variance among the input data (*39*). In this study,

we used a variant known as behavioural-PLS, where brain measurements (logged Jacobian values at the voxel level) and behavioural variables (derived from MWM and NOR tests, intervention assignment, and demographics) served as input data. Using behavioural data as input for PLS, even in the absence of significant differences in behavioral analysis, proves to be a useful approach; PLS facilitates dimensionality reduction while preserving essential information. This may reveal connections that are not readily apparent when examining separate variables. We did not include mice in groups that received the combined intervention due to missing behavioural data (see Materials and Methods, 'Partial Least Squares analysis').

PLS treats each of the two input matrices, here behaviour and brain measurements, as "blocks" and iteratively transforms them to find the maximum overlap between the two (maximized shared variance) (*40*). For details on these transformations, refer to McIntosh and Misic, 2013 (*41*). PLS produces several latent variables (LV), made up of a certain brain pattern and a given behavioural pattern, that together explain a percentage of the covariance among the data. The significance of the LVs was assessed by permutation and the standard errors and confidence intervals were calculated using bootstrap resampling. A bootstrap ratio (BSR) is calculated at the voxel level and is thresholded to identify significant regions and create the brain pattern that correlates to the behavioural pattern inside each LV (see Statistical Analysis, 'Partial Least Squares analysis').

In this study, we obtained 45 LVs, equivalent to the number of behavioural variables analyzed. However, only the first four LVs (LV1-4) were statistically significant based on permutation testing (LV1 p= 0.0170, LV2 p=0.0010, LV3 p= 0.0010, LV4 p= 0.0013). These LVs explained 29.36%, 13.44%, 12.46%, and 7.68% of the covariance respectively, see Fig. S8 for a plot showing the significance and covariance explained for the 45 LVs.

LV1 explained 29.36% of the covariance (Fig. S9-A). LV1 was characterized by an increased volume (positive BSR) in the cerebellum, olfactory bulbs, and hippocampus. This brain pattern correlated with being wild-type mice, having lower body weight, and performing well in memory tests. In summary, LV1 represented the healthiest of the mice, which had no predisposition to develop any characteristics of AD, as the 3xTgAD mice did.

LV2 (Fig. S9-B) accounted for 13.44% of the covariance. It was characterized by a volume decrease (negative BSR) in the cerebellum and hippocampus and a widespread volume increase in the caudoputamen and cortex areas. This brain pattern was associated with being male, being 3xTgAD mice, having higher weight, and having worse memory. Therefore, LV2 represented mice at risk of developing AD characteristics (3xTgAD mice).

LV3 accounted for 12.46% of the covariance (Fig. 7) and showed increased volume in the hippocampus and parts of the cerebellum. This pattern positively correlated with a low-fat diet

and physical activity interventions, negatively correlated with no intervention and higher weight, and was linked to better cognitive outcomes for the MWM test, e.g. correlated with better performance as measured by the GCM and passthrough (indicators of spatial memory). LV3 captured the features of mice that received either physical activity or a low-fat diet, showing a brain pattern that was similar to those brain patterns we identified with the volumetric and voxel-wise analysis.

LV4 accounted for 7.68% of the covariance explained (Fig. S9-C), this was characterized by a widespread volume decline and higher volume in the olfactory bulbs, which correlated with being wild-type. This LV did not correlate with another variable that could have added more information as to the group of mice it was capturing.

Given that LV3 was the only LV that captured a correlation between brain volume changes and the intervention strategies, we decided to explore the 'brain scores', a measure derived from PLS. Brain scores reflect how much each mouse expressed the brain pattern produced by the LV; e.g. a mouse with a higher brain score is highly represented by the brain pattern observed in LV3. The PLS analysis also output behaviour scores that gave a measure per mouse of how well the behavioural pattern of the LV represented the given mouse. Brain scores were plotted against weight, GCM, and number of pass-throughs. A negative relationship between brain scores for LV3 and weight ($r = -0.35$; Fig. S10) indicated that mice with higher weight were less likely to exhibit the brain pattern represented by LV3. This suggested that the structural brain features associated with LV3 (higher volumes in the cerebellum and hippocampus) were inversely related to body weight. We also obtained a negative relationship for GCM ($r = -0.27$, Fig. S11-A), which suggested that the brain pattern represented by LV3 was associated with improved memory function, (e.g. lower GCM values). Lastly, when plotting brain scores against the number of pass-throughs, the positive correlation ($r = 0.42$, Fig. S11-B) showed that higher brain scores were linked to increased passthrough counts, indicating better learning and memory of the platform's location.

Lastly, we plotted brain scores per group (Fig. 7-C) and found higher brain scores for groups that received interventions, meaning the brain pattern of LV3 was better representing mice in the physical activity and low-fat diet groups. Plots of brain scores for other LVs support that LV1 is better representing WT mice (Fig. S12-A), LV2 is better representing 3xTgAD mice, with a higher brain score median for 3xTgAD mice that didn't receive any intervention (Tg_HighFat, Fig. S12-B), and LV4 is capturing features of WT mice (Fig. S12-C) that are particularly strong in olfactory bulbs (Fig. S9-C).

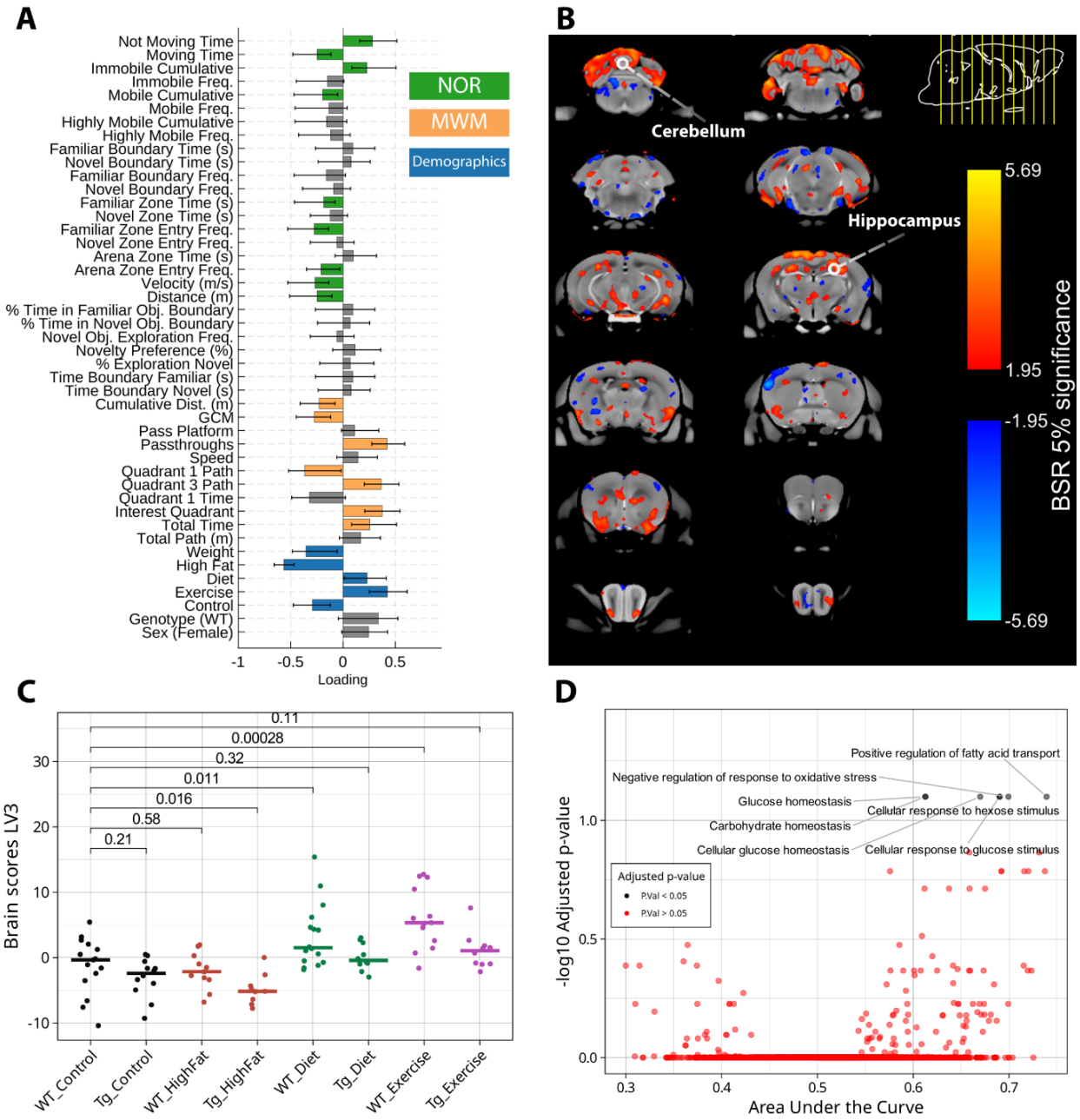


**Fig. 7. PLS results for LV3 and gene enrichment analysis.** We show the behavioural pattern (**A**) that maximally covaries with the brain pattern (**B**) for LV3. For the behavioural data (**A**), variables from the NOR (in green), the MWM (in yellow), and the treatment groups or demographics (in blue) are shown. The bars show how much each behaviour contributes to the pattern of LV3 (x-axis: loading values). Singular value decomposition estimated the size of the bars, whereas confidence intervals were estimated by bootstrapping. Bars with error bars that crossed the zero line are not significant (in gray). (**B**) brain loading BSR are overlaid on the population average. BSR thresholded to 95% confidence interval (N=96 mice with complete

data). (**C**) Brain scores and medians per group for LV3. We observe higher brain scores in WT_Diet and WT_Exercise groups. Statistics are pair-wise t-test comparisons corrected with FDR. (**D**) Scatter plot showing significant modules found with SGEA. We identify 7 terms associated with top-ranked genes; these are genes that better correlate with the brain loading from LV3, have an area under the curve > 0.5, and are statistically significant (P-value<0.05). The significant terms are: negative regulation of response to oxidative stress (GO:1902883), glucose homeostasis (GO:0042593), carbohydrate homeostasis (GO:0033500), cellular glucose homeostasis (GO:0001678), cellular response to hexose stimulus (GO:0071331), cellular response to glucose stimulus (GO:0071333) and positive regulation of fatty acid transport (GO:2000193).

**Biological processes underlying the anatomical signature of LV3**

Given that the brain pattern of LV3 was associated with intervention strategies, we proposed that these interventions contributed to the brain pattern observed. This hypothesis is grounded in prior evidence that these interventions influence neuroanatomy (*19*, *20*, *42*) and metabolic pathways (*43*, *44*).

Under this assumption, we aimed to uncover the biological mechanisms that could be driving the LV3 brain pattern. To achieve this, we correlated the brain pattern with gene expression data from the Allen Institute's Mouse Brain Atlas (*45–47*). Genes were ranked by Spearman correlation followed by a spacial gene enrichment analysis (SGEA) to examine the enrichment of these genes within gene ontology (GO) terms (*48*) (see Materials and Methods, 'Spatial Gene Enrichment Analysis'). Here, GO terms correspond to biological processes linked to the top-ranked genes (*49*). In summary, the objective was to identify GO terms whose genes' expression patterns resemble the LV3 spatial brain pattern. We used statistical methods to evaluate the significance of this enrichment (see Statistical Analysis, 'Spatial Gene Enrichment Analysis').

Seven significant GO terms emerged (Fig. 7-D), highlighting key biological processes: 1) Negative regulation of response to oxidative stress—a process that reduces, prevents, or stops responses to oxidative stress (GO:1902883); 2) Glucose homeostasis—the maintenance of a stable internal glucose level within an organism or cell (GO:0042593); 3) Carbohydrate homeostasis—the regulation of stable carbohydrate levels within an organism (GO:0033500); 4) Cellular glucose homeostasis—the maintenance of glucose levels specifically within a cell (GO:0001678); 5-6) Cellular response to hexose/glucose stimulus—a process where cells alter their state or activity in response to hexose/glucose (GO:0071331 and 0071333); and 7) Positive regulation of fatty acid transport—a process that increases or activates the transport of fatty acids (GO:2000193).

The ancestry analysis of cellular response to glucose stimulus (GO:0071333) (*50*) revealed hierarchical relationships with carbohydrate homeostasis, glucose homeostasis, cellular glucose homeostasis, and cellular response to hexose stimulus. This suggests a coordinated regulatory network controlling glucose metabolism. In contrast, negative regulation of oxidative stress response and positive regulation of fatty acid transport were independent, indicating distinct pathways.

**Discussion**

While there are no disease-modifying treatments for AD, reducing the incidence of new cases through intervention strategies emerges as an important approach to addressing this global challenge (*51*). In this manuscript, we leveraged neuroimaging techniques to study the effects of a high-fat diet on the mouse brain and how intervention strategies including physical activity, a low-fat diet, or their combination, can counteract these effects. We collected a unique dataset encompassing 156 mice, divided into similar groups per genotype (3xTgAD and WT). In these groups, we evaluated weight, behaviour, and neuroanatomy, and used multivariate analysis to find hidden patterns in the data that led to the discovery of possible biological processes behind the impact of exercise and low-fat diet. Although our focus was not to understand how interventions delay or prevent dementia, our findings support their role in promoting brain health by reversing the effects of a high-fat diet in mice.

To evaluate neuroanatomical changes, we used volumetric and DBM analyses. DBM provides insights into subtle, region-specific deformations that volumetric measures may overlook. We found that genotype itself affected the cortex volume as found before in previous work done in our lab (*18*, *35*). In addition, we found pronounced changes in the olfactory bulbs, hippocampus, caudoputamen, and cerebellum, which replicate work from our lab aimed at characterizing the neuroanatomical trajectories of the 3xTgAD mice (*35*). We also found that a high-fat diet affected the hippocampus and cerebellum (in WT mice only), structures that have been shown to present modifications with a high-fat diet or obesity in both rodents and humans, impacting neurogenesis and synaptic plasticity in the hippocampus in rodents (*52*, *53*), and causing decreased volume in the left cerebellum in both adults and children (*54*, *55*). The lack of effects of a high-fat diet on 3xTgAD mice could be attributed to their genetic predisposition, which is linked to neuroanatomical vulnerabilities (*35*, *56*, *57*). This genetic vulnerability could explain why we found smaller volumes for the cerebellum and hippocampus in 3xTgAD mice.

Peak voxels allowed us to understand the effect of intervention strategies. In many instances, we noticed that the interventions drove the Jacobian values (which indicate volume expansion or contraction) to comparable levels as the control groups, or even exceeded those levels for the groups that received a combined intervention. Nonetheless, we must take into account that there

are biological mechanisms that contribute to these voxel-wise changes (*58*), which we did not aim to explore with the approaches implemented here. In animal models, a high-fat diet increases microglial activation (*59*), causes changes in hippocampal mitochondrial morphology, and leads to a reduction in synapse number (*60*). On the contrary, voluntary physical activity has been shown to increase dendritic complexity in the dentate gyrus (*61*), regulate synaptic transmission in the hippocampus (*62*), promote angiogenesis after an ischemic injury (*63*), and increase the volume of both hippocampus and cerebellar regions (*21*), while a low-fat diet has not been well studied in terms of effects at the microscopic level. Of interest, a study evaluating the same interventions as in this work found that they mitigate high-fat diet related amyloid-β accumulation and memory impairments in transgenic mice that overexpress the human amyloid-β precursor protein (APP) in the hippocampus (*64*).

We studied the 3xTgAD mice to model AD-relevant susceptibility to risk factors. These mice have transgenes for APPSWE and PS1M146V along with an extra mutation associated with frontotemporal dementia, tauP301L, resulting in the formation of both Aβ plaques and neurofibrillary tangles in the model (*65*). In 3xTgAD mice, it is expected to find few amyloid-β plaques and some tau phosphorylation in the hippocampal regions by 6 months of age (*66*, *67*), which could explain why we didn't find group differences in univariate analyses of behavioural variables derived from NOR and MWM tests at 6 months; perhaps the effects of these AD-related proteins or the effects of intervention strategies wasn't strong enough to present behavioural group differences at 6 months in this study.

Furthermore, when using the multivariate approach, we observed a brain pattern characterized by growth in the cerebellum and hippocampus that negatively correlated with a high-fat diet, and positively correlated with physical activity and diet interventions. First, it is important to highlight that we were able to delineate these structures with an analysis that ignored neuroanatomy. Second, this finding highlights the value of using a multivariate analytical approach to uncover complex interdependencies between the data that might be overlooked with univariate methods. With thousands of voxels, PLS revealed low-dimensionality features highlighting states of interest (here, intervention strategies). Interpreting data that has undergone dimension reduction remains a topic of discussion (*68–70*). However, the bootstrap method used here allowed for the identification of a statistically significant brain pattern that encodes potential biological meaning, as exposed by our further SGEA analysis.

Previous work correlating spatial neuroanatomical changes to spatial patterns of gene expression data found that changes in neuroanatomy can help pinpoint genes responsible for the observed phenotypes (*71*). Here, the SGEA analysis correlating gene expression data to the PLS LV3 brain pattern uncovers GO terms associated with biological processes such as glucose homeostasis and positive regulation of fatty acid transport. Here, five out of the seven significant terms are related to glucose homeostasis. These processes have been discovered through other studies, for

example, a study in a transgenic model for AD (and WT counterpart) found that a low-fat diet reversed the alterations in glucose metabolism in mice fed a high-fat diet, taking glucose to comparable levels as control mice (fed with a low-fat diet) (*72*). Another study found that a high-fat diet enhanced glucose intolerance in a transgenic model of AD, reversible with the injection of insulin (*73*). Whereas, to our knowledge, regulation of response to oxidative stress and regulation of fatty acid transport are not extensively studied in this context, exercise could promote these processes (*74–76*), for example, a study found that exercise decreased reactive oxygen species in rats fed with a high-fat diet (*77*).

The data we gathered indicates a potential function of the cerebellum in feeding circuits that merits further investigation. Traditionally, the cerebellum has been associated with motor control, however, new evidence supports that it might also be related to cognitive functions (*78*). Previous research shows a decrease in the neuronal density in both the cerebellar cortex and deep nuclei of the cerebellum in 3xTgAD mice (*56*). This suggests a genetic vulnerability in 3xTgAD mice, which may contribute to the pronounced cerebellar changes observed. Another study found that APP and apoptosis-related molecules (e.g. caspases) increase in the cerebellum of WT mice after only 7 days on a high-fat diet (*79*). A study on children found that physical fitness was associated with larger volumes in some regions of the cerebellum (*80*). Another study found that children who perceived an inability to control how much is eaten had lower grey matter in the parahippocampal gyrus and the left cerebellar lobule VI (*81*). It has been proposed that since eating behaviours are influenced by predictions (e.g., hunger before a meal, or expectations of food taste) and feedback (e.g., satiety after eating), the cerebellum might be involved in managing prediction errors in these domains, adjusting responses to align with sensory feedback and expectations across motor, cognitive, and affective processes (*82*).

In terms of the limitations of this work, here we used a high-fat diet with 60% of calories coming from fat. A high-fat diet formulated for mice typically consists of 40-60% fat, with different combinations of saturated and unsaturated fatty acids (*83*). In the U.S., the percentage of total calories coming from fat ranges between 30-40% (*84*), whereas the last report from 2000 indicates that the Canadian population consumes around 30% of calories coming from fat (*85*). Therefore, animal models fed with a high-fat diet considerably exceed these values, leading to a pronounced effect of a high-fat diet that might not resemble what we can find in humans. Additionally, our findings related to biological processes behind interventions should be confirmed. Future work should address this question as well as the best timing for the initiation of these interventions.

In summary, our findings underscore the potential of diet and exercise interventions to counteract the adverse effects of a high-fat diet on the brain, particularly in regions like the cerebellum and hippocampus. Additionally, they highlight the necessity for more research to investigate the underlying mechanisms and the applicability of these findings to human health.

## Materials and Methods

### Animals

All animal experiments were carried out following the Canadian Council on Animal Care and approved by the McGill University Animal Care Committee (Montreal, QC, Canada). Male and female homozygous 3xTgAD mice (https://www.jax.org/strain/004807, RRID:MMRRC_034830-JAX) and non-transgenic Wild-Type (WT) B6129SF2J mice (https://www.jax.org/strain/101045, RRID:IMSR_JAX:101045) were acquired through the Mutant Mouse Resource and Research Center (MMRRC) and were bred on an F2 hybrid cross between C57BL/6J females (B6) and 129S1/SvImJ males (129S). The 3xTgAD mice have a knocked-in PS1M146V mutation at the mouse PSI locus and two human transgenes: APPSwe and tauP301L (*65*). The PS1M146V and APPSwe mutations affect the processing of the amyloid-beta precursor protein (APP) into Amyloid-beta (*86*), while TauP301L induces tauopathy (*87*). It has been reported that 3xTgAD exhibits cognitive impairments related to memory retention at four months of age, accumulating intraneuronal amyloid plaques in the cortex, hippocampus, and amygdala (*88*). Other studies have reported cognitive impairment, amyloid plaques, and neurofibrillary tangles in the hippocampus at six months of age (*66*). A recent characterization of 3xTgAD mice reported a shift in timing in plaques and tangles appearance, with a more substantial impact on females due to estrogen-regulated gene promoters (*89*, *90*). Mice were bred in an in-house colony, and their offspring were weaned during the fourth week after birth. The offspring were housed in groups of three to four mice per cage at the Douglas Mental Health University Institute's Animal Facility (Montreal, QC, Canada) in standard housing conditions (12h light/dark cycle, with lights on at 8:00 hrs.). Mice received ad libitum access to standard chow (control diet) and water until interventions started at two months of age.

### Experimental design

All mice were on a standard diet from weaning until two months of age (2016 Teklad Global 16% Protein Rodent Diet, Inotiv, Madison, Wisconsin USA), containing 4% fat from soybean oil, formulated for growth and maintenance. At two months, 80% of both 3xTgAD and WT mice were randomly assigned to an obesity-inducing high-fat diet (Teklad high-fat diet TD.06414 with 60% of kcal from fat, primarily lard, Inotiv, Madison, Wisconsin USA), while the remaining mice continued on a low-fat diet (Teklad Purified Control Diet TD.08806 with 10.5% of kcal from fat, primarily soybean oil and lard, Inotiv, Madison, Wisconsin USA). From four to six months, mice fed a low-fat diet continued on it and served as controls (groups: WT_Control and Tg_Control), while a subset of mice on the high-fat diet remained in it (WT_Highfat and Tg_Highfat). During this same period (4-6 months), to assess the reversibility of the induced

obesity, the rest of the mice fed with the high-fat diet were randomly assigned to either a low-fat diet (groups: WT_Diet and Tg_Diet), physical activity (groups: WT_Exercise and Tg_Exercise) or the combination of both interventions (groups: WT_Both and Tg_Both). In the physical activity groups, mice had access to a running wheel for voluntary activity. Food intake was not monitored due to the difficulties in obtaining accurate measurements (*91*), and mice were not placed in isolation to measure wheel use because this introduces the effect of social isolation (*92*). Weekly weight measurements were collected for at least 18 data points per mouse from two to six months of age (n=157 mice with 18 measurements each). T1-weighted MRI scans were acquired at two, four, and six months, followed by behavioural testing with the MWM and NOR tests at six months. Out of the initial 165 mice involved (around 16 mice per group and a nearly equal number of males and females), 9 died or were sacrificed before the final neuroimaging timepoint, primarily due to fighting (four males and one female), hydrocephalus (one male, one female), and MnCl2 injections (two males). Male aggression, especially after wheel introduction, contributed to attrition. Fighting caused an entire cage of 3xTgAD mice on the combined intervention to be sacrificed. Fig. 1 shows the experimental workflow, and Table 1 shows the timeline at which each group received their respective diets and the N per group at each scanning time point.

| Group | Genotype | Intervention | Diet 0-2 mo. | Diet 2-4 mo. | Diet 4-6 mo. | TP 1 N (males, females) | TP 2 N (males, females) | TP 3 N (males, females) |
|---|---|---|---|---|---|---|---|---|
| **WT_Control** | WT | None | Standard | Low-fat | Low-fat | 16 (7, 9) | 15 (6, 9) | 15 (6, 9) |
| **WT_HighFat** | WT | None | Standard | High-fat | High-fat | 15 (9, 6) | 15 (9, 6) | 15 (9, 6) |
| **WT_Diet** | WT | Diet | Standard | High-fat | Low-fat | 17 (10, 7) | 17 (10, 7) | 17 (10, 7) |
| **WT_Exercise** | WT | Exercise | Standard | High-fat | High-fat | 18 (12, 6) | 18 (12, 6) | 18 (12, 6) |
| **WT_Both** | WT | Both | Standard | High-fat | Low-fat | 17 (10, 7) | 17 (10, 7) | 17 (10, 7) |
| **Tg_Control** | 3xTgAD | None | Standard | Low-fat | Low-fat | 16 (6, 10) | 16 (6, 10) | 16 (6, 10) |
| **Tg_HighFat** | 3xTgAD | None | Standard | High-fat | High-fat | 16 (10, 6) | 16 (10, 6) | 16 (10, 6) |
| **Tg_Diet** | 3xTgAD | Diet | Standard | High-fat | Low-fat | 16 (6, 10) | 16 (6, 10) | 16 (6, 10) |
| **Tg_Exercise** | 3xTgAD | Exercise | Standard | High-fat | High-fat | 18 (11, 7) | 17 (10, 7) | 16 (9, 7) |
| **Tg_Both** | 3xTgAD | Both | Standard | High-fat | Low-fat | 16 (9, 7) | 13 (6, 7) | 10 (5, 5) |
| | | | | | Total = | 165 | 160 | 156 |

**Table 1. Number of mice per time point.** The table lists the different diets each group received during the experiment and the number of mice available at time point 1 (2 months of age), time point 2 (4 months of age), and time point 3 (6 months of age) when brain images were acquired. Table S1 lists the nutrient information for each diet.

### Magnetic Resonance Image acquisition

T1w MRI images were acquired at three time points, when mice were two, four, and six months old. These time points were selected to capture the neuroanatomy at baseline and before and after

interventions. Scans were collected using a 7T small animal scanner (Bruker Biospec 70/30 USR; 30-cm inner bore diameter) at the Douglas Mental Health University Institute (Montreal, QC, CA). Mice were prepared 24 hours before the scanning with a bicine-buffered solution of manganese (II) chloride (MnCl2) titrated with 1 M sodium hydroxide (NaOH; Sigma Aldrich, Switzerland) at a dosage of 62.5 mg/kg. MnCl2 enhances the contrast of T1w structural MRI scans due to the paramagnetism of Mn2+ that reduces the T1 relaxation time, enhancing the contrast between tissues (*93*, *94*). NaOH and bicine were added to mitigate the acidic environment caused by MnCl2, preventing tissue damage at the injection site and keeping the pH at about 7.4 (*95*). Dosage was calculated based on weight at baseline to avoid toxic doses in obese mice. High doses were observed to cause skin lesions in previous work from our group (*18*). The injection was administered to the intraperitoneal cavity to limit toxicity (*96*). Before the scanning, animals were anesthetized with isoflurane (Fresenius Kabi Canada Ltd, Richmond Hill, CA) at 5% and injected with 0.5 mL of 0.9% sterile sodium chloride physiological solution (Sigma Aldrich). During the scanning, mice were maintained under 1-2% isoflurane, with breathing rate monitored and maintained at 30-100 breaths per minute. The sequence used to acquire the scans was a 3-dimensional fast low-angle shot (3D FLASH), and the T1w MRI was taken with two averages (TR = 20 ms, TE = 4.5 ms, matrix size = 180 x 160 x 90, voxel dimensions = 100 µm isotropic, and flip angle = 20°) and fat suppression. Scans were collected with the Bruker 23 mm volumetric transmit/receive quadrature coil (*97*).

**Image processing**

Raw Digital Imaging and Communications in Medicine (DICOM) scans were converted to the Medical Imaging Net CDF (MINC) file format and preprocessed with a set of tools and libraries developed in our laboratory and at the Montreal Neurological Institute (MNI) freely available online (Minc-toolkit 1.9.16, RRID: SCR_014138). Preprocessing included stripping images of their native coordinate system, left-right flipping of images to compensate for the scanner's native radiological coordinate system, denoising using a patch-based non-local means filter previously validated (*98*), and affine registration to an average mouse template to produce a brain mask. N4ITK was used as an improved version of the N3 bias field correction algorithm for inhomogeneity correction at a minimum distance of 5 mm (*99*). Then, a de-scaled and de-sheared version of the affine registration was used to perform a rigid alignment of the scan to the mouse template space (*100*). Images were inspected using the Display visualization software of MINC tools. Quality control was performed for each time point. The inspection was mostly focused on the presence of hydrocephalus or motion-related artifacts. Of the 165 scans collected at timepoint one, 160 passed quality control; from the 160 scans collected at timepoint two, 148 passed; and from the 156 scans collected at timepoint three, 145 passed quality control. Therefore, we used 453 scans for further analysis.

**Volumetric analysis**

We performed a volumetric analysis on mice with at least one scan that passed quality control (total n=161 mice, 453 scans) to study whether the high-fat diet and intervention strategies impacted the neuroanatomy of 3xTgAD and wild-type mice. We parcellated the brain into 182 structures per hemisphere using the Multiple Automatically Generated Templates (MAGeT) brain segmentation algorithm (*101*). MAGeT first performs a non-linear transformation between the input data (T1w MRI scans) and the input atlas. Here, we used the DSURQE (Dorr-Steadman-Ullmann-Richards-Qiu-Egan) mouse brain atlas (*28–31*). The transforms obtained from the atlas to template registration are used to label each subject. The newly labeled scans are used as a template library, and pairwise non-linear transformation is performed to generate as many segmentations per subject as there are templates in the library. The set of labels is further subjected to a voting procedure at the voxel level, where the most voted label is selected for the final segmentation. Quality control of the outputs was performed by visually inspecting each segmentation overlaid on each mouse scan and verifying the labels matched the brain anatomy. Out of 453 segmentations, 385 passed quality control, corresponding to scans from 157 mice: 139 scans from the first timepoint, 116 scans from the second, and 130 scans from the third. Labels in the olfactory bulbs were not included in the analysis due to frequent artifacts in this region (For the list of labels in the olfactory bulb not included in the analysis, see Table S2). Volumes were computed from these segmentations.

**Deformation Based Morphometry analysis**

After our volumetric study, we aimed to analyze the changes in volume without any *a priori* on neuroanatomical boundaries. We applied a deformation-based analysis pipeline to model voxel-wise volume changes using the Jacobian determinant, which measures voxel contraction or expansion relative to a template (*34*, *102*). Scans from mice with at least two scans that passed quality control (n= 152 mice, 423 scans) served as input. To study overall brain differences, absolute Jacobians modeling the linear and non-linear transformations were generated using the two-level model-building toolkit Pydpiper (*103*). Scans were non-linearly registered to create a population-specific average template, followed by a group-wise registration to account for the longitudinal nature of our data (*103*). The non-linear registration was performed using the diffeomorphic MINC Advanced Normalization Tools (mincANTs) algorithm (*104*, *105*). The absolute Jacobians were log-transformed and blurred (0.2 mm full-width at half-maximum) to conform to Gaussian assumptions for statistical testing (*34*, *100*). For within-subject registration, an average representation of each specific subject's anatomy over time was created using a hierarchical multi-resolution registration strategy (*105*). These subject-specific averages served as inputs to build the group average and the common space for group-wise and longitudinal comparisons (*35*, *100*). We used the resampled absolute Jacobians adjusted for whole-brain size for all analyses. A Jacobian determinant exceeding 1 means that a voxel within the subject is

larger than the corresponding voxel in the population average. In contrast, Jacobians below 1 indicate a smaller voxel in the subject than the population average.

**Partial Least Squares analysis**

To study the relationship between voxel-wise changes and behavioural data, we ran a behaviour Partial Least Squares analysis (PLS) in Matlab 2022a (PLScmd software; Baycrest, Canada) as previously done in other work from our group (*106*). PLS can be used when the number of features (e.g. voxel-wise data) is higher than the number of observations (e.g. number of mice) and despite the presence of correlated variables (collinearity) (*107*). We constructed a matrix (X) made of voxel-wise Jacobian data from the last MRI scan collected (third timepoint, n= 96 mice). Another matrix (Y) was built with data from 45 variables, including demographics and behavioural data from the MWM and NOR tests. The matrix X and Y were correlated and subjected to a mathematical process (singular value decomposition) to obtain latent variables (LV). Only mice with complete data were included, this led to the exclusion of mice in the groups that received the combined intervention (Tg_Both and WT_Both). PLS produces as many LVs as there are variables in the behavioural data, in our case, 45. LVs can be interpreted as maximally covarying brain patterns and their associated behavioural factors (*108*). Behavioural variables used for partial least squares analysis were: 1) Demographic**:** sex, genotype, low-fat or high-fat diet, intervention type, no intervention, 2) Variables from Morris Water Maze: total path in meters, total time, time in quadrant of interest, time and distance in other quadrants, speed, count of passthroughs above the platform, passthroughs near the platform zone, GCM, cumulative time in the platform zone in milliseconds, 3) Variables from the novel object recognition test: time in the boundary of the novel object (seconds), time in the boundary of the familiar object (seconds), percentage of time of exploration of the novel object, preference for novelty, frequency in the novel object exploration, percentage of time of exploration in the boundary of the novel object, percentage of time of exploration in the boundary of the familiar object, distance (meters), velocity (milliseconds), frequency entering the zone of the arena, time spent in the zone of the arena (seconds), frequency entering the zone of the novel object, frequency entering the zone of the familiar object, time spent in the zone of the novel object (seconds), time spent in the zone of the familiar object (seconds), frequency entering the zone of the boundary of the novel object, frequency entering the zone of the boundary of the familiar object, time spent in the zone of the boundary of the novel object, time spent in the zone of the boundary of the familiar object, frequency of high-mobility, cumulative time of high-mobility, frequency in mobility, cumulative time of mobility, frequency in immobility, cumulative time immobile, moving time, not moving time.

**Spatial Gene Enrichment Analysis**

To assess the biological mechanisms underlying the brain pattern identified using PLS (latent variable 3), we conducted a Spatial Gene Enrichment Analysis (SGEA) in R/4.1.3. We utilized

gene expression data from the Allen Institute's Mouse Brain Atlas (*45*), which contains 4345 three-dimensional images of gene expression for 4082 unique genes acquired by immunohistochemistry on brain slices from adult (P56) male C57Bl/6 mice. Additionally, we used the high-resolution Allen Mouse Brain Common Coordinate Framework template (CCFv3, 200 µm voxel size) (*46*). Gene annotations for biological processes (modules) were drawn from the Gene Ontology (GO) consortium (MOUSE_GO_bp_no_GO_iea_symbol, with 15757 gene sets) (*109*), with genes inferred from electronic annotations. The gene expression images and CCFv3 template were realigned to RAS+ orientation and converted to the MINC format. Next, we conducted the SGEA analysis in R/4.1.3 using the brain-loading bootstrap ratio map from LV3 as the input. By spatially correlating the brain loading map with gene expression patterns, we identified gene expression profiles that correlate with the brain patterns. These genes were then ranked based on their correlation with the phenotype using Spearman correlation.

**Behavioural tests**

Novel Object Recognition (NOR) was performed one week after the third MRI scan, and the Morris water maze (MWM) test was performed two days after the NOR test. For the NOR test, on day zero, mice were placed in a cubic open field box (45 cm3) with bedding from their cage. Mice were allowed to explore for 10 min. On day one, mice were placed in the same box with bedding from their home cage, and they were allowed to explore two identical objects (4 cm3 each) for 10 min. The objects were spaced 20 cm apart. Mice were returned to their home cage, and one hour later, they returned to the test box with one object replaced with the novel object. Mice were given 10 minutes to explore. The location of the novel object was randomized (left or right side) and balanced across trials. The tests were conducted under a red light and an overhead camera. The camera recorded the test, and the resultant video clips were converted from DAV to AVI and further edited to last precisely 10 min. Videos were analyzed with Ethovision XT 12 Software. Only data from the test trial was used. During analysis, a boundary area around the object was set to 10 cm2. The exploration time was measured by summing up the time spent in the boundary area for both objects. Ideally, during the 10-minute test, mice should have an exploration time of 20 seconds (*23*). Mice with an exploration time below 20 seconds were not considered for the statistical analysis of NOR variables. However, they were included in the partial least squares analysis. To determine if mice spent more time around the novel object, the percentage of exploration in the boundary zone of the novel object was calculated. To do so, the time spent in the boundary area of the novel object was divided by the sum of the time spent in the boundary area of the novel and familiar object and multiplied by 100. Another variable of interest was the discrimination index, also known as the discrimination ratio (*24*). If positive, the discrimination ratio indicates more time spent exploring the novel object. A value of zero means equal time spent on both objects. This variable was calculated as the amount of time spent exploring the boundary zone of the novel object minus the amount of time spent exploring the

boundary zone of the familiar object, divided by the total amount of time spent exploring the boundary zone of both objects.

The MWM test was performed in a circular tank (120 cm in diameter) with water at 21-22 ℃. Water was made opaque by adding white, non-toxic tempera paint. There were three visual cues on the interior wall of the tank above the water line (in north, east, and southwest). An escape platform with a diameter of 15 cm was used. On day zero, mice were habituated with a trial where the escape platform was visible (1 cm above the water line). The anterior allowed the identification of apparent sensorimotor deficits. From day one to five, mice were trained six times by entering the tank with a non-visible escape platform always located in the southwest quadrant. During this training, mice entered the tank from one of three starting points (northeast, southwest, and southeast) in pseudorandom order. If the mice couldn't find the platform in 60 seconds, they were gently guided towards it. A failure was a training in which mice didn't find the platform within 60 seconds. On day six (probe day), a single trial was performed. In this trial, the escape platform was removed. Mice entered through the northeast point and were allowed 60 seconds to explore. Each trial was recorded with a mounted camera above the tank. However, some mice were recorded with a different camera due to software failure. Only data from probe day was used. Mice were excluded if they failed to find the platform in three of the six trainings. The data from the first camera was analyzed with tracking software (HVS Image Ltd). The data captured with the second camera was analyzed using a different software (Ethovision Noldus XT 12). Variables of interest were further analyzed, such as the average cumulative distance from the platform (also known as cumulative Gallagher's measure) and the number of pass-throughs (passages above the previous platform location). The cumulative distance from the platform is recognized as a solid measure of memory, and it has a good sensitivity to small differences in groups (*26*, *110*).

## Statistical Analysis

### Weight and behaviour

The weight data were analyzed with Linear Mixed Effects (LME) models in R (version 4.1.3) and the "effects" package, with weight as the dependent variable and group membership and sex as independent variables. Weeks since the change in diet were modeled as a third-degree polynomial, and a random intercept per mouse was allowed. Model: $Weight \sim Group*\text{poly}(Week,3) + Sex + (1|ID)$. behavioural data derived from the MWM and NOR were statistically assessed using two-tailed independent sample t-tests with FDR correction using stat_compare_means from ggpubr 0.6.0. Results were plotted using ggplot2 in R. The statistical comparisons were conducted for the following pairs: "WT_Control" versus "WT_HighFat", "WT_HighFat" versus "WT_Diet", "WT_HighFat" versus "WT_Exercise", "WT_HighFat" versus "WT_Both", "WT_Control" versus "Tg_HighFat", "Tg_Control" versus "Tg_HighFat",

"Tg_HighFat" versus "Tg_Diet", "Tg_HighFat" versus "Tg_Exercise", and "Tg_HighFat" versus "Tg_Both".

**Volumetric and deformation-based analyses**

The association between volume data derived from MAGeT and groups was evaluated with a hierarchical LME model with RMINC/v1.5.3.0 package for R (*111*). The model included volume per region as the dependent variable, an interaction between group and age in days, sex as an independent variable, and a random intercept allowed per mouse (*Volume* ~ *Group**poly(*Age*,2) + *Sex* + (*1*|*ID*)). The poly(*Age*,2) term allows the model to capture quadratic (second-degree polynomial) relationships between Age in days and volume while considering interaction effects with each group; data from the three time points was included. The linear mixed effects model output was corrected for multiple comparisons with a False Discovery Rate (FDR) with a 10% threshold (*33*). Results were plotted by overlaying the statistics map on top of the population average using functions available in RMINC. The plots display the linear terms of the interaction between group and age in days (*Group**poly(*Age*, 2)[1]), as the quadratic interaction didn't yield any significant results.
In the case of the deformation-based morphometry analysis, we assessed statistical significance by fitting an LME model at each voxel using the RMINC/v1.5.3.0 package for R (*111*). The model included logged absolute Jacobian determinants as the dependent variable, an interaction term between group and age in days, sex as an independent variable, and a random intercept allowed per mouse (*logged absolute Jacobian determinant* ~ *Group**poly(*Age*,2) + *Sex* + (*1*|*ID*)). Data from the three time points was included. The model outputs were corrected for multiple comparisons with FDR, with a 10% threshold. Results were plotted by overlaying the statistics map on top of the population average. Visualization of voxel-wise trajectories of peak voxels was done using RMINC and ggplot2. As in the case of the volumetric results, the plots display the linear terms of the interaction between group and age in days (*Group**poly(*Age*, 2)[1]), as the quadratic interaction didn't yield any significant results. When looking at the Jacobian values from the third time point, group comparisons were made using t-tests with FDR correction using stat_compare_means from ggpubr 0.6.0.

**Partial Least Squares Analysis**

The output LVs were statistically assessed by permutation testing (3000 tests), and the contribution of individual variables to each LV was assessed with bootstrap resampling to estimate standard errors and confidence intervals (3000 samples) (*112*). Bootstrap is a statistical resampling technique that creates several samples (with replacement) from the original dataset to assess the variability of the analysis. The bootstrap ratio (BSR) is calculated as the original weight/loading derived from the PLS, divided by the standard error of the weights or loadings obtained from the bootstrap resampling. A BSR is frequently compared with a standard normal

distribution (e.g., a threshold of 1.95 for a 95% confidence interval) to assess significance. BSRs are used to determine which brain areas significantly relate to behavioural measures inside a LV.

**Spatial Gene Enrichment Analysis**

For the SGEA analysis, we used the tmodUtest function (tmod/0.46.2 package in R) to assess significance. Genes were ranked based on their correlation with the phenotype (brain pattern) using Spearman correlation. Gene modules (groups of genes with shared biological functions) were selected from the GO consortium if they contained between 100 and 500 genes. For each module, we determine which of its genes appear in the ranked list and where they fall in the ranking. This step allowed us to assess whether certain modules are enriched with highly ranked genes (i.e., genes that are strongly correlated with the phenotype). The Mann-Whitney test was used to compute a U-statistic and p-values for the ranked gene list, with further transformation to the Area Under the Curve (AUC) to measure effect size. The significance of the AUC was tested by comparing the fold-change (enrichment) of each module against randomized AUC null distributions (*113*), with p-values adjusted using FDR correction.

**References**


1. S. A. Gale, D. Acar, K. R. Daffner, Dementia. *Am. J. Med.* **131**, 1161–1169 (2018).

2. World Health Organization, "Global status report on the public health response to dementia" in *Security Research Hub Reports* (2021; https://digitalcommons.fiu.edu/srhreports/health/health/65/).

3. T. Niccoli, L. Partridge, Ageing as a risk factor for disease. *Curr. Biol.* **22**, R741–52 (2012).

4. G. Livingston, J. Huntley, A. Sommerlad, D. Ames, C. Ballard, S. Banerjee, C. Brayne, A. Burns, J. Cohen-Mansfield, C. Cooper, S. G. Costafreda, A. Dias, N. Fox, L. N. Gitlin, R. Howard, H. C. Kales, M. Kivimäki, E. B. Larson, A. Ogunniyi, V. Orgeta, K. Ritchie, K. Rockwood, E. L. Sampson, Q. Samus, L. S. Schneider, G. Selbæk, L. Teri, N. Mukadam, Dementia prevention, intervention, and care: 2020 report of the Lancet Commission. *Lancet* **396**, 413–446 (2020).

5. W. C. Knowler, K. M. V. Narayan, R. L. Hanson, R. G. Nelson, P. H. Bennett, J. Tuomilehto, B. Schersten, D. J. Pettitt, Preventing non-insulin-dependent diabetes. *Diabetes* **44**, 483–488 (1995).

6. M. Tubiana, Cancer prevention. *Acta Oncol.* **38**, 689–694 (1999).

7. K. M. Rexrode, J. E. Manson, C. H. Hennekens, Obesity and cardiovascular disease. *Curr. Opin. Cardiol.* **11**, 490–495 (1996).

8. M. Baumgart, H. M. Snyder, M. C. Carrillo, S. Fazio, H. Kim, H. Johns, Summary of the evidence on modifiable risk factors for cognitive decline and dementia: A population-based perspective. *Alzheimers. Dement.* **11**, 718–726 (2015).

9. S.-Y. Huang, Y.-Z. Li, Y.-R. Zhang, Y.-Y. Huang, B.-S. Wu, W. Zhang, Y.-T. Deng, S.-D. Chen, X.-Y. He, S.-F. Chen, Q. Dong, C. Zhang, R.-J. Chen, J. Suckling, E. T. Rolls, J.-F. Feng, W. Cheng, J.-T. Yu, Sleep, physical activity, sedentary behavior, and risk of incident dementia: a prospective cohort study of 431,924 UK Biobank participants. *Mol. Psychiatry* **27**, 4343–4354 (2022).

10. E. Zotcheva, S. Bergh, G. Selbæk, S. Krokstad, A. K. Håberg, B. H. Strand, L. Ernstsen, Midlife Physical Activity, Psychological Distress, and Dementia Risk: The HUNT Study. *J. Alzheimers. Dis.* **66**, 825–833 (2018).

11. H. Hörder, L. Johansson, X. Guo, G. Grimby, S. Kern, I. Skoog, Author response: Midlife cardiovascular fitness and dementia: A 44-year longitudinal population study in women. *Neurology* **91**, 763 (2018).

12. E. Albanese, L. J. Launer, M. Egger, M. J. Prince, P. Giannakopoulos, F. J. Wolters, K. Egan, Body mass index in midlife and dementia: Systematic review and meta-regression analysis of 589,649 men and women followed in longitudinal studies. *Alzheimers. Dement.* **8**, 165–178 (2017).

13. N. Scarmeas, J. A. Luchsinger, N. Schupf, A. M. Brickman, S. Cosentino, M. X. Tang, Y. Stern, Physical activity, diet, and risk of Alzheimer disease. *JAMA* **302**, 627–637 (2009).

14. M. Milanski, G. Degasperi, A. Coope, J. Morari, R. Denis, D. E. Cintra, D. M. L. Tsukumo, G. Anhe, M. E. Amaral, H. K. Takahashi, R. Curi, H. C. Oliveira, J. B. C. Carvalheira, S. Bordin, M. J. Saad, L. A. Velloso, Saturated fatty acids produce an inflammatory response predominantly through the activation of TLR4 signaling in hypothalamus: implications for the pathogenesis of obesity. *J. Neurosci.* **29**, 359–370 (2009).

15. S. Khan, K. H. Barve, M. S. Kumar, Recent Advancements in Pathogenesis, Diagnostics and Treatment of Alzheimer's Disease. *Curr. Neuropharmacol.* **18**, 1106–1125 (2020).

16. I. García-García, A. Michaud, M. Dadar, Y. Zeighami, S. Neseliler, D. L. Collins, A. C. Evans, A. Dagher, Neuroanatomical differences in obesity: meta-analytic findings and their validation in an independent dataset. *Int. J. Obes.* **43**, 943–951 (2019).

17. E. Gómez-Apo, A. Mondragón-Maya, M. Ferrari-Díaz, J. Silva-Pereyra, Structural Brain Changes Associated with Overweight and Obesity. *J. Obes.* **2021**, 6613385 (2021).

18. C. P. E. Rollins, D. Gallino, V. Kong, G. Ayranci, G. A. Devenyi, J. Germann, M. M. Chakravarty, Contributions of a high-fat diet to Alzheimer's disease-related decline: A longitudinal behavioural and structural neuroimaging study in mouse models. *NeuroImage: Clinical* **21** (2019).

19. C. A. Raji, S. Meysami, S. Hashemi, S. Garg, N. Akbari, G. Ahmed, Y. G. Chodakiewitz, T.

D. Nguyen, K. Niotis, D. A. Merrill, R. Attariwala, Exercise-Related Physical Activity Relates to Brain Volumes in 10,125 Individuals. *J. Alzheimers. Dis.* **97**, 829–839 (2024).

20. B. M. Brown, J. de Frutos Lucas, T. Porter, N. Frost, M. Vacher, J. J. Peiffer, S. M. Laws, Non-Modifiable Factors as Moderators of the Relationship Between Physical Activity and Brain Volume: A Cross-Sectional UK Biobank Study. *J. Alzheimers. Dis.* **88**, 1091–1101 (2022).

21. L. S. Cahill, P. E. Steadman, C. E. Jones, C. L. Laliberté, J. Dazai, J. P. Lerch, B. Stefanovic, J. G. Sled, MRI-detectable changes in mouse brain structure induced by voluntary exercise. *Neuroimage* **113**, 175–183 (2015).

22. D. B. Reuben, S. Kremen, D. T. Maust, Dementia prevention and treatment: A narrative review. *JAMA Intern. Med.* **184**, 563–572 (2024).

23. L. M. Lueptow, Novel object recognition test for the investigation of learning and memory in mice. *J. Vis. Exp.* **2017**, 55718 (2017).

24. M. Antunes, G. Biala, The novel object recognition memory: Neurobiology, test procedure, and its modifications. Springer [Preprint] (2012). https://doi.org/10.1007/s10339-011-0430-z.

25. K. Bromley-Brits, Y. Deng, W. Song, Morris Water Maze test for learning and memory deficits in Alzheimer's disease model mice. *J. Vis. Exp.*, doi: 10.3791/2920 (2011).

26. I. T. Pereira, R. D. Burwell, Using the spatial learning index to evaluate performance on the water maze. *Behav. Neurosci.* **129**, 533–539 (2015).

27. H. R. Maei, K. Zaslavsky, C. M. Teixeira, P. W. Frankland, What is the most sensitive measure of water maze probe test performance? *Front. Integr. Neurosci.* **3**, 4 (2009).

28. A. E. Dorr, J. P. Lerch, S. Spring, N. Kabani, R. M. Henkelman, High resolution three-dimensional brain atlas using an average magnetic resonance image of 40 adult C57Bl/6J mice. *Neuroimage* **42**, 60–69 (2008).

29. K. Richards, C. Watson, R. F. Buckley, N. D. Kurniawan, Z. Yang, M. D. Keller, R. Beare, P. F. Bartlett, G. F. Egan, G. J. Galloway, G. Paxinos, S. Petrou, D. C. Reutens, Segmentation of the mouse hippocampal formation in magnetic resonance images. *Neuroimage* **58**, 732–740 (2011).

30. P. E. Steadman, J. Ellegood, K. U. Szulc, D. H. Turnbull, A. L. Joyner, R. M. Henkelman, J. P. Lerch, Genetic effects on cerebellar structure across mouse models of autism using a magnetic resonance imaging atlas. *Autism Res.* **7**, 124–137 (2014).

31. J. F. P. Ullmann, C. Watson, A. L. Janke, N. D. Kurniawan, D. C. Reutens, A segmentation protocol and MRI atlas of the C57BL/6J mouse neocortex. *Neuroimage* **78**, 196–203 (2013).

32. A. M. Fjell, K. B. Walhovd, L. T. Westlye, Y. Østby, C. K. Tamnes, T. L. Jernigan, A. Gamst, A. M. Dale, When does brain aging accelerate? Dangers of quadratic fits in cross-sectional studies. *Neuroimage* **50**, 1376–1383 (2010).

33. Y. Benjamini, D. Yekutieli, The Control of the False Discovery Rate in Multiple Testing under Dependency. *Ann. Stat.* **29**, 1165–1188 (2001).

34. M. K. Chung, K. J. Worsley, T. Paus, C. Cherif, D. L. Collins, J. N. Giedd, J. L. Rapoport, A. C. Evans, A Unified Statistical Approach to Deformation-Based Morphometry. doi: 10.1006/nimg.2001.0862 (2001).

35. V. Kong, G. A. Devenyi, D. Gallino, G. Ayranci, J. Germann, C. Rollins, M. M. Chakravarty, Early-in-life neuroanatomical and behavioural trajectories in a triple transgenic model of Alzheimer's disease. *Brain Struct. Funct.* **223**, 3365–3382 (2018).

36. S. Tullo, A. S. Miranda, E. Del Cid-Pellitero, M. P. Lim, D. Gallino, A. Attaran, R. Patel, V. Novikov, M. Park, F. H. Beraldo, W. Luo, I. Shlaifer, T. M. Durcan, T. J. Bussey, L. M. Saksida, E. A. Fon, V. F. Prado, M. A. M. Prado, M. M. Chakravarty, Neuroanatomical and cognitive biomarkers of alpha-synuclein propagation in a mouse model of synucleinopathy prior to onset of motor symptoms. *J. Neurochem.* **168**, 1546–1564 (2024).

37. S. Tullo, J. Park, D. Gallino, M. Park, K. Mar, V. Novikov, R. Sandoval Contreras, R. Patel, E. del Cid-Pellitero, E. A. Fon, W. Luo, I. Shlaifer, T. M. Durcan, M. A. M. Prado, V. F. Prado, G. A. Devenyi, M. M. Chakravarty, Sex-focused analyses of M83 A53T hemizygous mouse model with recombinant human alpha-synuclein preformed fibril injection identifies female resilience to disease progression: A combined magnetic resonance imaging and behavioural study, *bioRxiv* (2024). https://doi.org/10.1101/2024.05.24.595642.

38. A. Bussy, J. P. Levy, T. Best, R. Patel, L. Cupo, T. Van Langenhove, J. E. Nielsen, Y. Pijnenburg, M. L. Waldö, A. M. Remes, M. L. Schroeter, I. Santana, F. Pasquier, M. Otto, A. Danek, J. Levin, I. Le Ber, R. Vandenberghe, M. Synofzik, F. Moreno, A. de Mendonça, R. Sanchez-Valle, R. Laforce, T. Langheinrich, A. Gerhard, C. Graff, C. R. Butler, S. Sorbi, L. Jiskoot, H. Seelaar, J. C. van Swieten, E. Finger, M. C. Tartaglia, M. Masellis, P. Tiraboschi, D. Galimberti, B. Borroni, J. B. Rowe, M. Bocchetta, J. D. Rohrer, G. A. Devenyi, M. M. Chakravarty, S. Ducharme, GENetic Frontotemporal dementia Initiative (GENFI), Cerebellar and subcortical atrophy contribute to psychiatric symptoms in frontotemporal dementia. *Hum. Brain Mapp.* **44**, 2684–2700 (2023).

39. S. Rännar, F. Lindgren, P. Geladi, S. Wold, A PLS kernel algorithm for data sets with many variables and fewer objects. Part 1: Theory and algorithm. *J. Chemom.* **8**, 111–125 (1994).

40. R. W. Gerlach, B. R. Kowalski, H. O. A. Wold, Partial least-squares path modelling with latent variables. *Anal. Chim. Acta* **112**, 417–421 (1979).

41. A. R. McIntosh, B. Mišić, Multivariate statistical analyses for neuroimaging data. Annual Reviews Inc. [Preprint] (2013). https://doi.org/10.1146/annurev-psych-113011-143804.

42. D. E. A. Jensen, V. Leoni, M. C. Klein-Flügge, K. P. Ebmeier, S. Suri, Associations of

dietary markers with brain volume and connectivity: A systematic review of MRI studies. *Ageing Res. Rev.* **70**, 101360 (2021).

43. R. C. O. Macedo, H. O. Santos, G. M. Tinsley, A. Reischak-Oliveira, Low-carbohydrate diets: Effects on metabolism and exercise - A comprehensive literature review. *Clin. Nutr. ESPEN* **40**, 17–26 (2020).

44. O. S. Gondim, V. T. N. de Camargo, F. A. Gutierrez, P. F. de O. Martins, M. E. P. Passos, C. M. Momesso, V. C. Santos, R. Gorjão, T. C. Pithon-Curi, M. F. Cury-Boaventura, Benefits of regular exercise on inflammatory and cardiovascular risk markers in normal weight, overweight and obese adults. *PLoS One* **10**, e0140596 (2015).

45. E. S. Lein, M. J. Hawrylycz, N. Ao, M. Ayres, A. Bensinger, A. Bernard, A. F. Boe, M. S. Boguski, K. S. Brockway, E. J. Byrnes, L. Chen, L. Chen, T.-M. Chen, M. C. Chin, J. Chong, B. E. Crook, A. Czaplinska, C. N. Dang, S. Datta, N. R. Dee, A. L. Desaki, T. Desta, E. Diep, T. A. Dolbeare, M. J. Donelan, H.-W. Dong, J. G. Dougherty, B. J. Duncan, A. J. Ebbert, G. Eichele, L. K. Estin, C. Faber, B. A. Facer, R. Fields, S. R. Fischer, T. P. Fliss, C. Frensley, S. N. Gates, K. J. Glattfelder, K. R. Halverson, M. R. Hart, J. G. Hohmann, M. P. Howell, D. P. Jeung, R. A. Johnson, P. T. Karr, R. Kawal, J. M. Kidney, R. H. Knapik, C. L. Kuan, J. H. Lake, A. R. Laramee, K. D. Larsen, C. Lau, T. A. Lemon, A. J. Liang, Y. Liu, L. T. Luong, J. Michaels, J. J. Morgan, R. J. Morgan, M. T. Mortrud, N. F. Mosqueda, L. L. Ng, R. Ng, G. J. Orta, C. C. Overly, T. H. Pak, S. E. Parry, S. D. Pathak, O. C. Pearson, R. B. Puchalski, Z. L. Riley, H. R. Rockett, S. A. Rowland, J. J. Royall, M. J. Ruiz, N. R. Sarno, K. Schaffnit, N. V. Shapovalova, T. Sivisay, C. R. Slaughterbeck, S. C. Smith, K. A. Smith, B. I. Smith, A. J. Sodt, N. N. Stewart, K.-R. Stumpf, S. M. Sunkin, M. Sutram, A. Tam, C. D. Teemer, C. Thaller, C. L. Thompson, L. R. Varnam, A. Visel, R. M. Whitlock, P. E. Wohnoutka, C. K. Wolkey, V. Y. Wong, M. Wood, M. B. Yaylaoglu, R. C. Young, B. L. Youngstrom, X. F. Yuan, B. Zhang, T. A. Zwingman, A. R. Jones, Genome-wide atlas of gene expression in the adult mouse brain. *Nature* **445**, 168–176 (2007).

46. Q. Wang, S. L. Ding, Y. Li, J. Royall, D. Feng, P. Lesnar, N. Graddis, M. Naeemi, B. Facer, A. Ho, T. Dolbeare, B. Blanchard, N. Dee, W. Wakeman, K. E. Hirokawa, A. Szafer, S. M. Sunkin, S. W. Oh, A. Bernard, J. W. Phillips, M. Hawrylycz, C. Koch, H. Zeng, J. A. Harris, L. Ng, The Allen Mouse Brain Common Coordinate Framework: A 3D Reference Atlas. *Cell* **181**, 936–953.e20 (2020).

47. A. Arnatkevičiūtė, B. D. Fulcher, A. Fornito, A practical guide to linking brain-wide gene expression and neuroimaging data. *Neuroimage* **189**, 353–367 (2019).

48. M. J. M. F. Reijnders, R. M. Waterhouse, Summary visualizations of Gene Ontology terms with GO-Figure! *Front. Bioinform.* **1**, 638255 (2021).

49. S. Y. Rhee, V. Wood, K. Dolinski, S. Draghici, Use and misuse of the gene ontology annotations. *Nat. Rev. Genet.* **9**, 509–515 (2008).

50. EMBL-EBI, QuickGO. https://www.ebi.ac.uk/QuickGO/GTerm?id=GO:0071333.

51. N. A. Alwan, S. Stannard, A. Berrington, S. Paranjothy, R. B. Hoyle, R. K. Owen, S. D. S. Fraser, Risk factors for ill health: How do we specify what is “modifiable”? *PLOS Global Public Health* **4**, e0002887 (2024).

52. A. Lindqvist, P. Mohapel, B. Bouter, H. Frielingsdorf, D. Pizzo, P. Brundin, C. Erlanson-Albertsson, High-fat diet impairs hippocampal neurogenesis in male rats. *Eur. J. Neurol.* **13**, 1385–1388 (2006).

53. B. M. González Olmo, M. N. Bettes, J. W. DeMarsh, F. Zhao, C. Askwith, R. M. Barrientos, Short-term high-fat diet consumption impairs synaptic plasticity in the aged hippocampus via IL-1 signaling. *Npj Sci. Food* **7**, 35 (2023).

54. X. Ou, A. Andres, R. T. Pivik, M. A. Cleves, T. M. Badger, Brain gray and white matter differences in healthy normal weight and obese children. *J. Magn. Reson. Imaging* **42**, 1205–1213 (2015).

55. M. J. Herrmann, A.-K. Tesar, J. Beier, M. Berg, B. Warrings, Grey matter alterations in obesity: A meta-analysis of whole-brain studies. *Obes. Rev.* **20**, 464–471 (2019).

56. G. Esquerda-Canals, J. Marti, G. Rivera-Hernández, L. Giménez-Llort, S. Villegas, Loss of deep cerebellar nuclei neurons in the 3xTg-AD mice and protection by an anti-amyloid β antibody fragment. *MAbs* **5**, 660–664 (2013).

57. M. A. Gama Sosa, R. D. Gasperi, A. B. Rocher, A. C.-J. Wang, W. G. M. Janssen, T. Flores, G. M. Perez, J. Schmeidler, D. L. Dickstein, P. R. Hof, G. A. Elder, Age-related vascular pathology in transgenic mice expressing presenilin 1-associated familial Alzheimer’s disease mutations. *Am. J. Pathol.* **176**, 353–368 (2010).

58. N. Dieleman, H. L. Koek, J. Hendrikse, Short-term mechanisms influencing volumetric brain dynamics. *NeuroImage Clin.* **16**, 507–513 (2017).

59. E. M. Knight, I. V. A. Martins, S. Gümüsgöz, S. M. Allan, C. B. Lawrence, High-fat diet-induced memory impairment in triple-transgenic Alzheimer’s disease (3xTgAD) mice is independent of changes in amyloid and tau pathology. *Neurobiol. Aging* **35**, 1821–1832 (2014).

60. I. V. A. Martins, J. Rivers-Auty, S. M. Allan, C. B. Lawrence, Mitochondrial abnormalities and synaptic loss underlie memory deficits seen in mouse models of obesity and Alzheimer’s disease. *J. Alzheimers. Dis.* **55**, 915–932 (2017).

61. V. A. Redila, B. R. Christie, Exercise-induced changes in dendritic structure and complexity in the adult hippocampal dentate gyrus. *Neuroscience* **137**, 1299–1307 (2006).

62. S. S. Vaynman, Z. Ying, D. Yin, F. Gomez-Pinilla, Exercise differentially regulates synaptic proteins associated to the function of BDNF. *Brain Res.* **1070**, 124–130 (2006).

63. Y. Tang, Y. Zhang, M. Zheng, J. Chen, H. Chen, N. Liu, Effects of treadmill exercise on cerebral angiogenesis and MT1-MMP expression after cerebral ischemia in rats. *Brain*

*Behav.* **8**, e01079 (2018).

64. M. Maesako, K. Uemura, M. Kubota, A. Kuzuya, K. Sasaki, N. Hayashida, M. Asada-Utsugi, K. Watanabe, M. Uemura, T. Kihara, R. Takahashi, S. Shimohama, A. Kinoshita, Exercise is more effective than diet control in preventing high fat diet-induced β-amyloid deposition and memory deficit in amyloid precursor protein transgenic mice. *J. Biol. Chem.* **287**, 23024–23033 (2012).

65. S. Oddo, A. Caccamo, J. D. Shepherd, M. P. Murphy, T. E. Golde, R. Kayed, R. Metherate, M. P. Mattson, Y. Akbari, F. M. LaFerla, Triple-transgenic model of Alzheimer's disease with plaques and tangles: intracellular Abeta and synaptic dysfunction. *Neuron* **39**, 409–421 (2003).

66. R. Belfiore, A. Rodin, E. Ferreira, R. Velazquez, C. Branca, A. Caccamo, S. Oddo, Temporal and regional progression of Alzheimer's disease‐like pathology in 3xTg‐AD mice. *Aging Cell* **18** (2019).

67. A. Jullienne, M. V. Trinh, A. Obenaus, Neuroimaging of mouse models of Alzheimer's Disease. *Biomedicines* **10**, 305 (2022).

68. Z. Liu, K. J. Whitaker, S. M. Smith, T. E. Nichols, Improved interpretability of brain-behavior CCA with Domain-driven Dimension Reduction. *Front. Neurosci.* **16**, 851827 (2022).

69. Y. Tang, D. Chen, X. Li, Dimensionality reduction methods for brain imaging data analysis. *ACM Comput. Surv.* **54**, 1–36 (2022).

70. M. Danyluik, Y. Zeighami, A. Mukora, M. Lepage, J. Shah, R. Joober, B. Misic, Y. Iturria-Medina, M. M. Chakravarty, Evaluating permutation-based inference for partial least squares analysis of neuroimaging data, *bioRxiv* (2024). https://doi.org/10.1101/2024.08.02.606412.

71. D. J. Fernandes, J. Ellegood, R. Askalan, R. D. Blakely, E. Dicicco-Bloom, S. E. Egan, L. R. Osborne, C. M. Powell, A. Raznahan, D. M. Robins, M. W. Salter, A. S. Sengar, J. Veenstra-VanderWeele, R. M. Henkelman, J. P. Lerch, Spatial gene expression analysis of neuroanatomical differences in mouse models. *Neuroimage* **163**, 220–230 (2017).

72. J. M. Walker, S. Dixit, A. C. Saulsberry, J. M. May, F. E. Harrison, Reversal of high fat diet-induced obesity improves glucose tolerance, inflammatory response, β-amyloid accumulation and cognitive decline in the APP/PSEN1 mouse model of Alzheimer's disease. *Neurobiol. Dis.* **100**, 87–98 (2017).

73. M. Vandal, P. J. White, C. Tremblay, I. St-Amour, G. Chevrier, V. Emond, D. Lefrançois, J. Virgili, E. Planel, Y. Giguere, A. Marette, F. Calon, Insulin reverses the high-fat diet-induced increase in brain Aβ and improves memory in an animal model of Alzheimer disease. *Diabetes* **63**, 4291–4301 (2014).

74. D. Camiletti-Moirón, V. A. Aparicio, P. Aranda, Z. Radak, Does exercise reduce brain

oxidative stress? A systematic review. *Scand. J. Med. Sci. Sports* **23**, e202–12 (2013).

75. J. Souza, R. A. da Silva, D. da Luz Scheffer, R. Penteado, A. Solano, L. Barros, H. Budde, A. Trostchansky, A. Latini, Physical-exercise-induced antioxidant effects on the brain and skeletal muscle. *Antioxidants (Basel)* **11**, 826 (2022).

76. A. Liśkiewicz, M. Przybyła, A. Wojakowska, Ł. Marczak, K. Bogus, M. Nowacka-Chmielewska, D. Liśkiewicz, A. Małecki, J. Barski, J. Lewin-Kowalik, M. Toborek, Physical activity reduces anxiety and regulates brain fatty acid synthesis. *Mol. Brain* **13**, 62 (2020).

77. R. Molteni, A. Wu, S. Vaynman, Z. Ying, R. J. Barnard, F. Gómez-Pinilla, Exercise reverses the harmful effects of consumption of a high-fat diet on synaptic and behavioral plasticity associated to the action of brain-derived neurotrophic factor. *Neuroscience* **123**, 429–440 (2004).

78. L. F. Koziol, D. Budding, N. Andreasen, S. D'Arrigo, S. Bulgheroni, H. Imamizu, M. Ito, M. Manto, C. Marvel, K. Parker, G. Pezzulo, N. Ramnani, D. Riva, J. Schmahmann, L. Vandervert, T. Yamazaki, Consensus paper: the cerebellum's role in movement and cognition. *Cerebellum* **13**, 151–177 (2014).

79. C.-J. Xu, M.-Q. Li, Li-Zhao, W.-G. Chen, J.-L. Wang, Short-term high-fat diet favors the appearances of apoptosis and gliosis by activation of ERK1/2/p38MAPK pathways in brain. *Aging* **13**, 23133–23148 (2021).

80. P. Jalanko, L. Säisänen, E. Kallioniemi, M. Könönen, T. A. Lakka, S. Määttä, E. A. Haapala, Associations between physical fitness and cerebellar gray matter volume in adolescents. *Scand. J. Med. Sci. Sports* **34**, e14513 (2024).

81. A. L. Pearce, B. Fuchs, S. Adise, T. D. Masterson, N. Fearnbach, L. English, K. L. Keller, Loss of control eating in children is associated with altered cortical and subcortical brain structure. *Front. Psychol.* **14**, 1237591 (2023).

82. C. I. Iosif, Z. I. Bashir, R. Apps, J. Pickford, Cerebellar prediction and feeding behaviour. *Cerebellum* **22**, 1002–1019 (2023).

83. M. Lai, P. C. Chandrasekera, N. D. Barnard, You are what you eat, or are you? The challenges of translating high-fat-fed rodents to human obesity and diabetes. *Nutr. Diabetes* **4**, e135 (2014).

84. E. S. Ford, W. H. Dietz, Trends in energy intake among adults in the United States: findings from NHANES. *Am. J. Clin. Nutr.* **97**, 848–853 (2013).

85. K. Gray-Donald, L. Jacobs-Starkey, L. Johnson-Down, Food habits of Canadians: reduction in fat intake over a generation. *Can. J. Public Health* **91**, 381–385 (2000).

86. K. Duff, C. Eckman, C. Zehr, X. Yu, C.-M. Prada, J. Perez-tur, M. Hutton, L. Buee, Y. Harigaya, D. Yager, D. Morgan, M. N. Gordon, L. Holcomb, L. Refolo, B. Zenk, J. Hardy,

S. Younkin, Increased amyloid-β42(43) in brains of mice expressing mutant presenilin 1. *Nature* **383**, 710–713 (1996).

87. J. Lewis, E. McGowan, J. Rockwood, H. Melrose, P. Nacharaju, M. Van Slegtenhorst, K. Gwinn-Hardy, M. P. Murphy, M. Baker, X. Yu, K. Duff, J. Hardy, A. Corral, W. L. Lin, S. H. Yen, D. W. Dickson, P. Davies, M. Hutton, Neurofibrillary tangles, amyotrophy and progressive motor disturbance in mice expressing mutant (P301L)tau protein. *Nat. Genet.* **25**, 402–405 (2000).

88. L. M. Billings, S. Oddo, K. N. Green, J. L. McGaugh, F. M. LaFerla, Intraneuronal Abeta causes the onset of early Alzheimer's disease-related cognitive deficits in transgenic mice. *Neuron* **45**, 675–688 (2005).

89. D. I. Javonillo, K. M. Tran, J. Phan, E. Hingco, E. A. Kramár, C. da Cunha, S. Forner, S. Kawauchi, G. Milinkeviciute, A. Gomez-Arboledas, J. Neumann, C. E. Banh, M. Huynh, D. P. Matheos, N. Rezaie, J. A. Alcantara, A. Mortazavi, M. A. Wood, A. J. Tenner, G. R. MacGregor, K. N. Green, F. M. LaFerla, Systematic Phenotyping and Characterization of the 3xTg-AD Mouse Model of Alzheimer's Disease. *Front. Neurosci.* **15** (2022).

90. K. R. Sadleir, W. A. Eimer, S. L. Cole, R. Vassar, Aβ reduction in BACE1 heterozygous null 5XFAD mice is associated with transgenic APP level. *Mol. Neurodegener.* **10**, 1 (2015).

91. M. E. Starr, H. Saito, Age-Related Increase in Food Spilling by Laboratory Mice May Lead to Significant Overestimation of Actual Food Consumption: Implications for Studies on Dietary Restriction, Metabolism, and Dose Calculations. *J. Gerontol. A Biol. Sci. Med. Sci.* **67**, 1043 (2012).

92. J. Goh, W. Ladiges, Voluntary Wheel Running in Mice. *Curr. Protoc. Mouse Biol.* **5**, 283–290 (2015).

93. J. H. Lee, A. C. Silva, H. Merkle, A. P. Koretsky, Manganese-enhanced magnetic resonance imaging of mouse brain after systemic administration of MnCl2: Dose-dependent and temporal evolution of T1 contrast. *Magn. Reson. Med.* **53**, 640–648 (2005).

94. J. Yang, Q. Li, Manganese-Enhanced Magnetic Resonance Imaging: Application in Central Nervous System Diseases. *Front. Neurol.* **11**, 143 (2020).

95. Y. Seo, K. Satoh, K. Watanabe, H. Morita, A. Takamata, T. Ogino, M. Murakami, Mn-bicine: A low affinity chelate for manganese ion enhanced MRI. *Magn. Reson. Med.* **65**, 1005–1012 (2011).

96. Y. T. Kuo, A. H. Herlihy, P. W. So, K. K. Bhakoo, J. D. Bell, In vivo measurements of T1 relaxation times in mouse brain associated with different modes of systemic administration of manganese chloride. *J. Magn. Reson. Imaging* **21**, 334–339 (2005).

97. C. Anastassiadis, Effects of a high-fat diet and an exercise-based rescue on neuroanatomy in the triple-transgenic mouse model of Alzheimer's disease. (2020).

98. P. Coupe, P. Yger, S. Prima, P. Hellier, C. Kervrann, C. Barillot, An optimized blockwise nonlocal means denoising filter for 3-D magnetic resonance images. *IEEE Trans. Med. Imaging* **27**, 425–441 (2008).

99. N. J. Tustison, B. B. Avants, P. A. Cook, Y. Zheng, A. Egan, P. A. Yushkevich, J. C. Gee, N4ITK: Improved N3 Bias Correction. doi: 10.1109/TMI.2010.2046908 (2010).

100. D. Gallino, G. A. Devenyi, J. Germann, E. Guma, C. Anastassiadis, M. M. Chakravarty, Longitudinal assessment of the neuroanatomical consequences of deep brain stimulation: Application of fornical DBS in an Alzheimer's mouse model. *Brain Res.* **1715**, 213–223 (2019).

101. M. M. Chakravarty, P. Steadman, M. C. van Eede, R. D. Calcott, V. Gu, P. Shaw, A. Raznahan, D. L. Collins, J. P. Lerch, Performing label-fusion-based segmentation using multiple automatically generated templates. *Hum. Brain Mapp.* **34**, 2635–2654 (2013).

102. J. C. Lau, J. P. Lerch, J. G. Sled, R. M. Henkelman, A. C. Evans, B. J. Bedell, Longitudinal neuroanatomical changes determined by deformation-based morphometry in a mouse model of Alzheimer's disease. *Neuroimage* **42**, 19–27 (2008).

103. M. Friedel, M. C. van Eede, J. Pipitone, M. Mallar Chakravarty, J. P. Lerch, Pydpiper: A flexible toolkit for constructing novel registration pipelines. *Front. Neuroinform.* **8**, 67 (2014).

104. B. B. Avants, N. J. Tustison, G. Song, P. A. Cook, A. Klein, J. C. Gee, A Reproducible Evaluation of ANTs Similarity Metric Performance in Brain Image Registration. *Neuroimage* **54**, 2033 (2011).

105. B. B. Avants, N. Tustison, G. Song, Others, Advanced normalization tools (ANTS). *Insight J.* **2**, 1–35 (2009).

106. E. Guma, P. do C. Bordignon, G. A. Devenyi, D. Gallino, C. Anastassiadis, V. Cvetkovska, A. Barry, E. Snook, J. Germann, C. M. T. Greenwood, B. Misic, R. C. Bagot, M. M. Chakravarty, Early or late gestational exposure to maternal immune activation alters neurodevelopmental trajectories in mice: an integrated neuroimaging, behavioural, and transcriptional study. *Biol. Psychiatry*, doi: 10.1016/j.biopsych.2021.03.017 (2021).

107. R. D. Cramer III, Partial Least Squares (PLS): Its strengths and limitations. *Perspect. Drug Discov. Des.* **1**, 269–278 (1993).

108. A. R. McIntosh, F. L. Bookstein, J. V. Haxby, C. L. Grady, Spatial pattern analysis of functional brain images using partial least squares. *Neuroimage* **3**, 143–157 (1996).

109. Gene Ontology Consortium, Gene Ontology Consortium: going forward. *Nucleic Acids Res.* **43**, D1049–56 (2015).

110. C. V. Vorhees, M. T. Williams, Morris water maze: Procedures for assessing spatial and related forms of learning and memory. *Nat. Protoc.* **1**, 848–858 (2006).

111. J. Lerch, C. Hammill, M. van Eede, D. Cassel, J. Nikelski, Y. Yee, M. Friedel, N. Wang, G. Devenyi, RMINC: Statistical Tools for Medical Imaging NetCDF (MINC) Files. [Preprint] (2017). http://mouse-imaging-centre.github.io/RMINC.

112. A. R. McIntosh, N. J. Lobaugh, Partial least squares analysis of neuroimaging data: applications and advances. *Neuroimage* **23 Suppl 1**, S250–63 (2004).

113. B. D. Fulcher, A. Arnatkeviciute, A. Fornito, Overcoming false-positive gene-category enrichment in the analysis of spatially resolved transcriptomic brain atlas data. *Nat. Commun.* **12**, 2669 (2021).

**Acknowledgments**

**Funding:**
Healthy Brains Healthy Lives (CLG)
Fonds de Recherche du Québec - Santé (CLG, CA, MU)
Tanz Centre for Research on Neurodegenerative Diseases, University of Toronto, Toronto, CA. (CA)

**Author contributions:**
Conceptualization: CA, MMC
Data curation: CA
Formal analysis: CLG, CA
Investigation: CA, MP, MU, DG
Resources: MMC
Software: GAD, YY
Supervision: MMC
Visualization: CLG
Writing – original draft: CLG
Writing – review & editing: CLG, CA, MU, DG, GAD, MMC

**Competing interests:** The authors declare they have no competing interest.

**Data and materials availability:** The data that support the findings of this study are openly available in Zenodo at doi: 10.5281/zenodo.14907093.